Spontaneous emission in the optical microscopic cavity

F. De Martini, M. Marrocco, and P. Mataloni

Dipartimento di Fisica, Università "La Sapienza," Roma, 00185 Italy

L. Crescentini

Dipartimento di Fisica, Università de L'Aquila, L'Aquila, 67100 Italy

R. Loudon

Physics Department, University of Essex, Colchester, C04 3SQ, England

(Received 6 August 1990)

The quantum theory of the spontaneous emission (SpE) from an active microscopic cavity (microcavity) is given with emphasis on mirror separations of the order of the optical wavelength. The theory is based on a complete set of orthonormal-mode functions that include both transverse polarizations and span the infinite three dimensional space that pervades and surrounds the microcavity. SpE rates for different active-dipole orientations and cavity configurations are calculated. The SpE pulse shape detected outside the cavity is shown to be generally nonexponential. A detailed computer simulation of the process is presented on the basis of the given theory in the perspective of our experiment, for a cavity terminated by mirrors bearing either metal- or semiconductor-multilayered coatings. We then report an extensive experimental verification of the theory by adopting an Eu-dibenzoylmethane complex as active medium with SpE from the $^5D_0$-$^7F_2$ line at $\lambda = 6111$ Å, under coherent uv excitation at $\lambda_p = 3547$ Å. The results show evidence of "SpE inhibition" and "enhancement," of nonexponential decay of SpE signals, and of competition with superradiance and stimulated emission. Finally we report the results of an experimental test of the algorithm adopted in all computer calculations of the optical parameters of the multilayered structures used for cavity confinement.

I. INTRODUCTION

The problem of the interaction of atoms or molecules with the radiation field in its quantum ground state and in the presence of electromagnetic boundaries has attracted in the past a great deal of attention both on the theoretical[1,2] and experimental sides.[3] In recent times spontaneous-emission (SpE) enhancement-inhibition processes have been investigated in the microwave, infrared zones of the spectrum mostly by macroscopic cavity structures. The realization by our laboratory in Rome of the "microscopic cavity" (microcavity) and its application to SpE studies had added new features to this field of investigation often referred to as "cavity QED".[4] The optical frequency of the field interacting with atoms in the cavity prevents any stimulated-emission (StE) effect due to the residual Planck's radiation, which is mostly effective at far-infrared, microwave, and larger wavelengths. Moreover, the Casimir-type *extreme* vacuum confinement realized by this device leads to novel atom-field interaction processes as the competition of SpE with StE in *thresholdless-laser* dynamics[5] and to the recently reported evidence of *transverse* interatom quantum correlations.[6] The early sections of the present paper give a detailed quantum theory of SpE in a microcavity with the explicit evaluation of the SpE rates. Section II derives the traveling-wave modes of the cavity. In contrast to much of the earlier work, our calculations are based on a complete set of spatial modes that cover all of space, in-cluding the interior of the cavity and the exterior regions that extend to infinite distances on either side. The radiation field is quantized in terms of these modes in Sec. III, and the SpE rates are derived in Sec. IV. The results cannot be evaluated analytically in the general case, but they include various special cases and contact is made with expressions that have previously been derived for some of these. Section V gives the radiated-field operator for emitting atoms placed inside the cavity with detection outside it. There it is shown that SpE in a microcavity is a highly anisotropic process requiring a careful consideration of the mode orientation over which the detection is carried out. Section VI is devoted to the analytic evaluation of the generally nonexponential decay curves detected outside the cavity. These sections are followed by a detailed computer simulation of the process of SpE in conditions close to those of our experiment. Then, in Sec. VIII the description of the experiment and the experimental results is given for a microcavity terminated both by metal mirrors and by semiconductor-layered mirrors. The results of a detailed experimental test of the algorithm adopted in the computer simulation are also reported in the Appendix.

II. TRAVELING WAVE-MODES OF A FABRY-PÉROT CAVITY

In order to calculate the SpE rate of an atom in a Fabry-Pérot (FP) cavity, we first determine the appropriate spatial modes for quantization of the electromagnetic

field. The forms of the modes for propagation perpendicular to the plane mirrors of the cavity have been studied by Ley and Loudon.[7] We have generalized this work to cover all spatial directions. The geometrical details of the cavity are illustrated in Fig. 1. The z axis is taken normal to the mirrors with its origin in the middle of the cavity. The mirrors are assumed to have infinite extents in the xy plane. As represented in the figure, multiple reflections couple together waves of wave vectors:

$$\mathbf{k}_+ = k(\sin\Theta\cos\Phi, \sin\Theta\sin\Phi, \cos\Theta)$$

$$\mathbf{k}_- = k(\sin\Theta\cos\Phi, \sin\Theta\sin\Phi, -\cos\Theta) , \tag{2.1}$$

for $(0 \leq \Theta \leq \frac{1}{2}\pi)$. Four distinct spatial modes can be constructed from contributions with the same two wave vectors. For each set of polar angles, Θ and Φ, there are two transverse polarization directions whose unit vectors are chosen to be

$$\epsilon(\mathbf{k}_+, 1) = \epsilon(\mathbf{k}_-, 1) = (\sin\Phi, -\cos\Phi, 0) , \tag{2.2}$$

$$\epsilon(\mathbf{k}_+, 2) = (\cos\Theta\cos\Phi, \cos\Theta\sin\Phi, -\sin\Theta) ,$$

$$\epsilon(\mathbf{k}_-, 2) = (\cos\Theta\cos\Phi, \cos\Theta\sin\Phi, \sin\Theta) , \tag{2.3}$$

where the $\mathbf{k}_+$ and $\mathbf{k}_-$ designations indicate the polarizations of the respective wave-vector contributions. It is convenient to indicate the polarizations in (2.2) and (2.3) by an index $j = 1, 2$. The complex reflection and transmission coefficients r_{1j}, t_{1j} and r_{2j}, t_{2j} of the cavity mirrors are generally different for the two polarizations and depend on the polar angle Θ.[8] They are assumed to have the following unitary lossless properties, for all values of Θ:

$$|r_{1j}|^2 + |t_{1j}|^2 = |r_{2j}|^2 + |t_{2j}|^2 = 1 , \tag{2.4}$$

$$r_{1j}^* t_{1j} + r_{1j} t_{1j}^* = r_{2j}^* t_{2j} + r_{2j} t_{2j}^* = 0 , \tag{2.5}$$
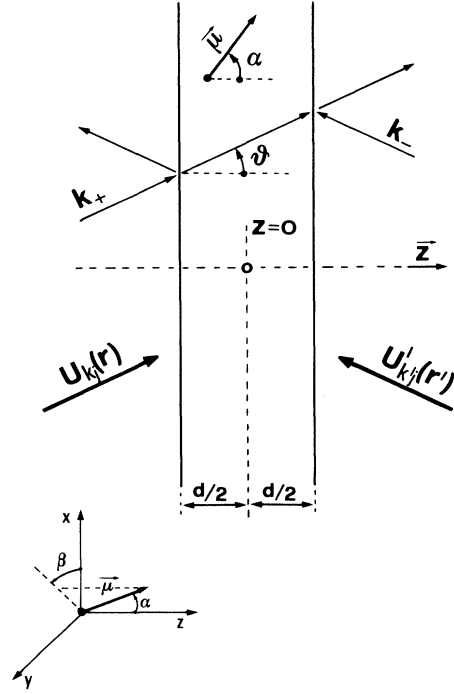

FIG. 1. Geometry of the Fabry-Pérot microcavity showing the two kinds of modes and the geometrical orientation of the dipole μ. Mirrors labeled by 1 and 2 in the text are represented, respectively, at the left and right in the figure.

where r_{1j}^* and t_{1j}^* are complex conjugates (c.c.) of r_{1j} and t_{1j}. Optical propagation within the mirrors is not important for the present study, and we accordingly ignore their internal mode structure. For each pair of coupled wave vectors $\mathbf{k}_+, \mathbf{k}_-$ designated by $\mathbf{k}$ for brevity, and for each transverse polarization there are two distinct mode functions corresponding to incoming plane waves of unit amplitude that are incident respectively from the negative and positive z sides of the cavity. The forms of these functions are obtained, as usual in Fabry-Pérot theory, by summing the geometric series resulting from the multiple reflections in the mirrors.[9] The two kinds of spatial dependence are thus given as follows:

Mode function $U_{\mathbf{k}j}(\mathbf{r})$

$\mathbf{k}_+$	$\mathbf{k}_-$	z
$\exp(i\mathbf{k}_+\cdot\mathbf{r})$	$R_{\mathbf{k}j}\exp(i\mathbf{k}_-\cdot\mathbf{r})$	$-\infty < z < -\frac{1}{2}d$
$t_{1j}\exp(i\mathbf{k}_+\cdot\mathbf{r})/D_j$	$t_{1j}r_{2j}\exp(i\mathbf{k}_-\cdot\mathbf{r}+ikd\cos\Theta)/D_j$	$-\frac{1}{2}d < z < +\frac{1}{2}d$
$T_{\mathbf{k}j}\exp(i\mathbf{k}_+\cdot\mathbf{r})$	0	$+\frac{1}{2}d < z < +\infty$

$$\tag{2.6}$$

Mode function $U'_{\mathbf{k}j}(\mathbf{r})$

$\mathbf{k}_+$	$\mathbf{k}_-$	z
$T'_{\mathbf{k}j}\exp(i\mathbf{k}_-\cdot\mathbf{r})$	0	$-\infty < z < -\frac{1}{2}d$
$t_{2j}\exp(i\mathbf{k}_-\cdot\mathbf{r})/D_j$	$t_{2j}r_{1j}\exp(i\mathbf{k}_+\cdot\mathbf{r}+ikd\cos\Theta)/D_j$	$-\frac{1}{2}d < z < +\frac{1}{2}d$
$\exp(i\mathbf{k}_-\cdot\mathbf{r})$	$R'_{\mathbf{k}j}\exp(i\mathbf{k}_+\cdot\mathbf{r})$	$-\frac{1}{2}d < z < +\infty$

$$\tag{2.7}$$

where the expressions in each row of (2.6) and (2.7) represent, as shown in Fig. 1, the plane-wave mode functions propagating in the space portions indicated at the right-hand side (rhs) and excited for the sets U_{kj}, U'_{kj} by the waves $\exp(i\mathbf{k}_+ \cdot \mathbf{r}), \exp(i\mathbf{k}_- \cdot \mathbf{r})$, respectively. In (2.6) and (2.7) the various quantities are defined as

$$D_j \equiv [1 - r_{1j}r_{2j}\exp(2ikd\cos\Theta)] , \tag{2.8}$$

$$R_{kj} = [r_{1j}\exp(-ikd\cos\Theta)$$
$$+ r_{2j}(t_{1j}^2 - r_{1j}^2)\exp(ikd\cos\Theta)]/D_j , \tag{2.9}$$

$$T_{kj} \equiv T'_{kj} = t_{1j}t_{2j}/D_j , \tag{2.10}$$

$$R'_{kj} \equiv [r_{2j}\exp(-ikd\cos\Theta)$$
$$+ r_{1j}(t_{2j}^2 - r_{2j}^2)\exp(ikd\cos\Theta)]/D_j . \tag{2.11}$$

The last three quantities represent the reflection and transmission coefficients of the cavity as a whole. It is not difficult to show, with the use of (2.4) and (2.5), that they satisfy

$$|R_{kj}| = |R'_{kj}| , \tag{2.12}$$

$$|R_{kj}|^2 + |T_{kj}|^2 = |R'_{kj}|^2 + |T'_{kj}|^2 = 1 , \tag{2.13}$$

$$R_{kj}^* T'_{kj} + R'_{kj} T_{kj}^* = 0 . \tag{2.14}$$

These properties ensure the normalization and orthogonality of the two modes that have the same wave vectors and polarizations and the general relations are

$$\int d\mathbf{r}\,\boldsymbol{\epsilon}(\mathbf{k},j)\cdot\boldsymbol{\epsilon}(\mathbf{k}',j')U_{kj}(\mathbf{r})U'^*_{k'j'}(\mathbf{r}) = 0 , \tag{2.15}$$

$$\int d\mathbf{r}\,\boldsymbol{\epsilon}(\mathbf{k},j)\cdot\boldsymbol{\epsilon}(\mathbf{k}',j')U_{kj}(\mathbf{r})U^*_{k'j'}(\mathbf{r}) = (2\pi)^3\delta_{jj'}\delta(\mathbf{k}-\mathbf{k}') , \tag{2.16}$$

together with the identical normalization integral for the primed mode function (2.7). The modes (2.6) and (2.7) form a complete set of functions for all of space, including the interior of the cavity and the exterior regions on either side. They allow calculations to be made of the SpE rates and radiated-field operators for atoms that are excited in cavities whose mirrors both transmit nonzero fractions of the emitted intensity. In addition, as will be shown in Sec. IV, they reproduce known results for SpE in cavities where one or both of the mirrors is or are perfect reflectors. Thus in the limiting case of a perfectly reflecting closed cavity, the traveling-wave mode functions used here reproduce results ordinarily obtained with standing-wave modes, while in the opposite extreme of an absent cavity, the mode functions (2.6) and (2.7) taken to-

gether produce the usual complete set of plane wave in infinite free space. In intermediate conditions the modes form a convenient basis for general calculations, and they are free of the potential limitations inherent in modes restricted to exterior regions of finite extent, or to only one side of the cavity.

III. FIELD QUANTIZATION

The electromagnetic field is quantized by the introduction of mode creation and destruction operators. The operators for the modes with spatial functions $U_{kj}(\mathbf{r})$ and $U'_{kj}(\mathbf{r})$ are denoted $\hat{a}^\dagger_{kj}, \hat{a}_{kj}$ and $\hat{a}'^\dagger_{kj}, \hat{a}'_{kj}$, respectively, where $j = 1,2$ indicates the choice of mode polarization, (2.2) or (2.3). With $\mathbf{k}$ taken to be a continuous variable, the operators satisfy the commutation relations,

$$[\hat{a}_{kj}, \hat{a}^\dagger_{k'j'}] = [\hat{a}'_{kj}, \hat{a}'^\dagger_{k'j'}] = \delta_{jj'}\delta(\mathbf{k}-\mathbf{k}')$$
$$[\hat{a}_{kj}, \hat{a}'^\dagger_{k'j'}] = [\hat{a}'_{kj}, \hat{a}^\dagger_{k'j'}] = 0 . \tag{3.1}$$

The electromagnetic field quantization now proceeds in the usual way, and we need quote only the main results.[7,10] The Heisenberg electric-field operator is conveniently separated into two parts:

$$\hat{\mathbf{E}}(\mathbf{r},t) = \hat{\mathbf{E}}^+(\mathbf{r},t) + \hat{\mathbf{E}}^-(\mathbf{r},t) , \tag{3.2}$$

where

$$\hat{\mathbf{E}}^+(\mathbf{r},t) = i\int d\mathbf{k}\sum_j (\hbar kc/16\pi^3\epsilon_0)^{1/2}\boldsymbol{\epsilon}(\mathbf{k},j)$$
$$\times [U_{kj}(\mathbf{r})\hat{a}_{kj} + U'_{kj}(\mathbf{r})\hat{a}'_{kj}]$$
$$\times \exp(-ickt) \tag{3.3}$$

and $\hat{\mathbf{E}}^-(\mathbf{r},t)$ is given by the Hermitian-conjugate (H.c.) expression. In writing out the field operators explicitly, the polarization vectors, given by (2.2) and (2.3), are those associated with the wave vectors $\mathbf{k}_-$ or $\mathbf{k}_+$ appropriate to the corresponding terms in the mode functions, given by (2.6) and (2.7). Because of the way in which wave-vector space is divided into two half spaces by the cavity the three-dimensional integral in (3.3) is

$$\int d\mathbf{k} = \int_0^\infty dk\int_0^{(1/2)\pi}d\Theta\int_0^{2\pi}d\Phi\,k^2\sin\Theta . \tag{3.4}$$

The normal-ordered part of the free-field Hamiltonian is

$$\hat{\mathbf{H}}_0 = \int d\mathbf{k}\,\hbar ck\sum_j (\hat{a}^\dagger_{kj}\hat{a}_{kj} + \hat{a}'^\dagger_{kj}\hat{a}'_{kj}), \quad j = 1,2 \tag{3.5}$$

and the Hamiltonian for interaction of the field with an atomic electric-dipole transition of matrix element $\boldsymbol{\mu}$ located at position $\mathbf{r}_0$ inside the cavity is

$$\hat{\mathbf{H}}_I = i\int d\mathbf{k}\sum_j (\hbar ck/16\pi^3\epsilon_0)^{1/2}[\exp(-ickt)/D_j]$$

$$\times \{\hat{a}_{kj}[\boldsymbol{\epsilon}(\mathbf{k}_+,j)t_{1j}\exp(i\mathbf{k}_+\cdot\mathbf{r}_0) + \boldsymbol{\epsilon}(\mathbf{k}_-,j)t_{1j}r_{2j}\exp(i\mathbf{k}_-\cdot\mathbf{r}_0 + ikd\cos\Theta)]$$

$$+ \hat{a}'_{kj}[\boldsymbol{\epsilon}(\mathbf{k}_-,j)t_{2j}\exp(i\mathbf{k}_-\cdot\mathbf{r}_0) + \boldsymbol{\epsilon}(\mathbf{k}_+,j)t_{2j}r_{1j}\exp(i\mathbf{k}_+\cdot\mathbf{r}_0 + ikd\cos\Theta)]\}\cdot\boldsymbol{\mu} + \text{H.c.} , \tag{3.6}$$

where (2.6) and (2.7) have been used.

IV. SPONTANEOUS-EMISSION RATE

The spontaneous-emission rate is calculated for the decay of an atom in the vacuum field of the cavity from an excited state of energy $\hbar c k_0$ to the atomic ground state. The experiments described below are carried out in regimes where the Markov approximation holds and the spontaneous-emission rate can accordingly be obtained by straightforward application of Fermi's golden rule (see further comments at the end of Sec. VI). We use the commutation properties (3.1) with the interaction Hamiltonian (3.6) and the result

$$(\mathbf{k}_+ - \mathbf{k}_-)\cdot\mathbf{r}_0 = 2kz_0\cos\Theta \ , \tag{4.1}$$

where z_0 is the z coordinate of the atomic position. The SpE rate for a molecular assembly belonging to a layer parallel to the mirrors, with coordinate $z = z_0$, of thickness dz, is then

$$\Gamma(z_0) = \int d\mathbf{k} \sum_j (k/8\pi^2\epsilon_0\hbar)(|\{\epsilon(\mathbf{k}_+,j)t_{1j} + \epsilon(\mathbf{k}_-,j)t_{1j}r_{2j}\exp[ik(d-2z_0)\cos\Theta]\}\cdot\boldsymbol{\mu}|^2$$

$$+ |\{\epsilon(\mathbf{k}_-,j)t_{2j} + \epsilon(\mathbf{k}_+,j)t_{2j}r_{1j}\exp[ik(d+2z_0)cos\Theta]\}\cdot\boldsymbol{\mu}|^2)\delta(k-k_0)/|D_j|^2 \ . \tag{4.2}$$

It is convenient to calculate separately the contributions to the SpE rate from the components of the transition dipole moment $\boldsymbol{\mu}$ parallel and perpendicular to the cavity mirrors. For the parallel contribution, we assume with no loss of generality that $\boldsymbol{\mu}$ is parallel to the x axis, so that (2.2) and (2.3) give

$$\epsilon(\mathbf{k}_+,1)\cdot\boldsymbol{\mu} = \epsilon(\mathbf{k}_-,1)\cdot\boldsymbol{\mu} = \mu\sin\Phi \quad \epsilon(\mathbf{k}_+,2)\cdot\boldsymbol{\mu} = \epsilon(\mathbf{k}_-,2)\cdot\boldsymbol{\mu} = \mu\cos\Theta\cos\Phi \ . \tag{4.3}$$

The k and Φ integrations, as defined in (3.4), can now be performed, and with the Θ integral simplified by a change of variable to $C \equiv \cos\Theta$, the emission rate is

$$\Gamma_\parallel(z_0) = (3\Gamma_0/8)\int_0^1 dC\{[(1-|r_{11}|^2)|1+r_{21}\exp(2iw_-)|^2 + (1-|r_{21}|^2)|1+r_{11}\exp(2iw_+)|^2]|D_1|^{-2}$$

$$+ [(1-|r_{12}|^2)|1+r_{22}\exp(2iw_-)|^2 + (1-|r_{22}|^2)|1+r_{12}\exp(2iw_+)|^2]|C/D_2|^2\} \ , \tag{4.4}$$

where

$$\Gamma_0 \equiv k_0^3\mu^2/(3\pi\epsilon_0\hbar) \equiv (T_0)^{-1} \tag{4.5}$$

is the usual free-space SpE rate,[10] k is replaced by k_0 in the expression (2.8) for D_j, (2.4) has been used to express the emission rate entirely in terms of the Θ-dependent mirror reflectivities, and

$$w_+ \equiv k_0(\tfrac{1}{2}d + z_0)C, \quad w_- \equiv k_0(\tfrac{1}{2}d - z_0)C, \quad w \equiv k_0 dC, \quad C \equiv \cos\Theta \ . \tag{4.6}$$

The SpE rate for a dipole moment perpendicular to the mirrors, or parallel to the z axis, is calculated in a similar fashion. The polarizations (2.2) and (2.3) now give

$$\epsilon(\mathbf{k}_+,1)\cdot\boldsymbol{\mu} = \epsilon(\mathbf{k}_-,1)\cdot\boldsymbol{\mu} = 0, \quad \epsilon(\mathbf{k}_+,2)\cdot\boldsymbol{\mu} = -\epsilon(\mathbf{k}_-,2)\cdot\boldsymbol{\mu} = -\mu\sin\Theta \ , \tag{4.7}$$

and the emission rate (4.2) becomes

$$\Gamma_\perp(z_0) = (3\Gamma_0/4)\int_0^1 dC(1-C^2)|1-r_{12}r_{22}\exp(2iw)|^{-2}[(1-|r_{12}|^2)|1-r_{22}\exp(2iw_-)|^2 + (1-|r_{22}|^2)|1-r_{12}\exp(2iw_+)|^2] \tag{4.8}$$

after partial integration as before. The above expressions simplify in various special cases. We consider briefly some of these before applying them to the interpretation of our experimental results.[8]

Free space. Complete removal of the cavity mirrors is accomplished by taking

$$r_{1j} = r_{2j} = 0, \quad t_{1j} = t_{2j} = 1 \ . \tag{4.9}$$

The integrations in (4.4) and (4.8) then become trivial, with the expected results $\Gamma_\parallel(z_0) = \Gamma_\perp(z_0) = \Gamma_0 \equiv (T_0)^{-1}$, and T_0 is the free-space SpE lifetime.

Half space. We consider the half space formed by removing mirror 2 and making mirror 1 perfectly reflecting, so that

$$r_{1j} = -1, \quad r_{2j} = 0, \quad t_{1j} = 0, \quad t_{2j} = 1 \ . \tag{4.10}$$

The integrations in (4.4) and (4.8) can again be performed and the results are

$$\Gamma_\parallel(z_0) = \Gamma_0(1 - (\tfrac{3}{2})\{[\sin(2w_0)/2w_0](1 - \tfrac{1}{4}w_0^{-2})$$

$$+ \cos(2w_0)/(2w_0)^2\}) \ , \tag{4.11}$$

$$\Gamma_\perp(z_0) = \Gamma_0\{1 + 3[\sin(2w_0)/2w_0 - \cos(2w_0)]/(2w_0)^2\} \ , \tag{4.12}$$

and

$$w_0 \equiv k_0(\tfrac{1}{2}d + z_0) \tag{4.13}$$

is the distance of the atom from the remaining mirror. These rate expressions agree with Morawitz[11] and with Eqs. (11) and (13) of Philpott.[12]

Symmetrical cavity. In this case we put

$$r_{1j} = r_{2j} = r_j = -|r_j|, \quad t_{1j} = t_{2j} = t_j = i|t_j| \ . \tag{4.14}$$

It is not possible to perform the integrals in (4.4) and (4.8)

but the integrands can be put in forms more convenient for computation, as

$$\Gamma_\parallel(z_0) = (3\Gamma_0/4) \int_0^1 dC \, [F_1(C) + C^2 F_2(C)] \tag{4.15}$$

and

$$\Gamma_\perp(z_0) = (3\Gamma_0/2) \int_0^1 dC \, (1 - C^2) G_2(C) \tag{4.16}$$

where

$$F_1(C) \equiv [(1 - |r_1|)^2 + 2|r_1|(\sin^2 w_- + \sin^2 w_+)] / [1 - |r_1|^2 + 4(|r_1|^{-2} - 1)^{-1} \sin^2 w] \ ,$$

$$G_2(C) \equiv [(1 - |r_2|)^2 + 2|r_2|(\cos^2 w_- + \cos^2 w_+)] / [1 - |r_2|^2 + 4(|r_2|^{-2} - 1)^{-1} \sin^2 w] \ ,$$

and $F_2(C)$ is obtained by substituting r_1 by r_2 in the expression of $F_1(C)$. These expressions can be combined to give the SpE rate for a transition whose dipole moment has an isotropic spatial distribution as

$$\Gamma(z_0) = [2\Gamma_\parallel(z_0) + \Gamma_\perp(z_0)]/3$$

$$= \tfrac{1}{2}\Gamma_0 \int_0^1 dC (F_1(C) + [1 - |r_2|^2 + 4(|r_2|^{-2} - 1)^{-1} \sin^2 w]^{-1}$$

$$\times \{(1 + |r_2|)^2 - 2|r_2|[\sin^2 w_- + \sin^2 w_+ + 2C^2 \cos w \cos(2k_0 C z_0)]\}) \ . \tag{4.17}$$

High-Q cavity. Take a symmetrical cavity, as specified by (4.14) but in addition consider the limit

$$|r_j| \to 1 \quad |t_j| \to 0 \ . \tag{4.18}$$

The Airy-function denominators in the integrands of the SpE rates can then be expressed as sums of δ functions according to

$$1/|D_j|^2 \equiv [(1 - |r_j|^2)^2 + 4|r_j|^2 \sin^2 w]^{-1}$$

$$\approx \sum_{n=0}^\infty \{[2|r_j|(w - n\pi)]^2 + (1 - |r_j|^2)^2\}^{-1}$$

$$\approx \{\pi/[2k_0 d|r_j|(1 - |r_j|^2)]\}$$

$$\times \left[\tfrac{1}{2}\delta(C) + \sum_{n=1}^\infty \delta(C - (n\pi/k_0 d)) \right] \ . \tag{4.19}$$

The integrals can now be performed, and the number of δ-function contributions is equal to the integer next greater than $k_0 d/\pi$. The SpE rates obtained in this way agree with expressions derived previously.[12-15] We do not repeat these expressions here, but only give the SpE rates for cavities so narrow that only one or two Airy-function peaks contribute. Thus (4.15)–(4.17) give

$$\Gamma_\parallel(z_0) = 0 \ ,$$

$$\Gamma_\perp(z_0) = 3\pi\Gamma_0/(2k_0 d) \ , \tag{4.20}$$

$$\Gamma(z_0) = \pi\Gamma_0/(2k_0 d) \ ,$$

for $0 < (k_0 d) < \pi$, and

$$\Gamma_\parallel(z_0) = (3\pi\Gamma_0/2k_0 d)[1 + (\pi/k_0 d)^2]\cos^2(\pi z_0/d) \ , \tag{4.21}$$

$$\Gamma_\perp(z_0) = (3\pi\Gamma_0/2k_0 d)$$

$$\times \{1 + 2[1 - (\pi/k_0 d)^2]\sin^2(\pi z_0/d)\} \ , \tag{4.22}$$

$$\Gamma(z_0) = (3\pi\Gamma_0/2k_0 d)$$

$$\times [1 + (2\pi^2/3k_0^2 d^2)\cos(2\pi z_0/d)] \tag{4.23}$$

for $0 < (k_0 d) < 2\pi$. Note that when $k_0 d$ exceeds π by an infinitesimal amount, (4.21) and (4.22) give

$$\Gamma_\parallel(z_0) = 3\Gamma_0 \cos^2(\pi z_0/d), \quad \Gamma_\perp(z_0) = 3\Gamma_0/2 \ , \tag{4.24}$$

in agreement with previous results.[13,16] The functions $\Gamma_\parallel(z_0)$ and $\Gamma_\perp(z_0)$ shown in Fig. 2 have been computer evaluated on the basis of the general formulas (4.15) and (4.16) by assuming that the reflectivities are independent of Θ and that fields undergo a Θ-independent phase change $\phi = \pi$ upon reflection. However, we should emphasize once again that the Θ dependence of field reflectivities, transmittivities, and phases which is realized in actual cases with *any* kind of mirror coating leads to quite different results for $\Gamma_\parallel(z_0)$ and $\Gamma_\perp(z_0)$ as shown by Fig. 3.[8] It is noteworthy that the method of calculation used here, in which the field modes are defined by (2.6) and (2.7) as plane waves of unit amplitude incident from *outside* the cavity, gives the same results as calculations for a perfectly reflecting cavity in which the field modes are taken to be standing waves *inside* the cavity.

Very narrow cavity, $d \approx 0$. The exponents in (4.4) and (4.8) can be set equal to zero for $k_0 d \ll 1$, and if we disregard the dependence on Θ of the reflection and transmission parameters of the mirrors, the integrals can then be evaluated to give.[8]

$$\Gamma_\parallel(0) = \Gamma_0(|t_1|^2 |1 + r_2|^2 + |t_2|^2 |1 + r_1|^2)/(2|1 - r_1 r_2|^2) \ , \tag{4.25}$$

$$\Gamma_\perp(0) = \Gamma_0(|t_1|^2 |1 - r_2|^2 + |t_2|^2 |1 - r_1|^2)/(2|1 - r_1 r_2|^2) \ . \tag{4.26}$$

These expressions simplify for the symmetrical cavity specified by (4.14) where

$$\Gamma_\parallel(0)=\Gamma_0(1-|r|)/(1+|r|) \; ,$$

$$\Gamma_\perp(0)=\Gamma_0(1+|r|)/(1-|r|) \; ,$$

(4.27)

consistent with (4.20) in the limit of a high-Q cavity.

Apart from the special cases of absent or perfectly reflecting mirrors, the transmission and reflection coefficients generally depend upon the magnitude and direction of the wave vector $\mathbf{k}$, as already said.[8] Thus in the expressions for SpE rates, the mirror reflection and transmission coefficient should strictly be shown as func-

tions of Θ as shown for metal mirrors by Fig. 17. Apart from the results of Fig. 2 the functional dependence on Θ of r_i, t_i, $i=1,2$, for metal-layered and multilayered mirrors will be accounted for rigorously in all computer calculations leading to the results reported in the present work.[8]

V. FIELD RADIATED BY AN EXCITED ATOM

Consider an experiment in which the SpE radiation from an atom at position $\mathbf{r}_0$ inside the cavity is observed at position $\mathbf{r}$ outside the cavity. The electric-field operator at position $\mathbf{r}$ at time t is obtained from (2.6), (2.7), and (3.3) as

$$\hat{\mathbf{E}}^+(\mathbf{r},t)=i\int d\mathbf{k}\sum_j (\hbar ck/16\pi^3\epsilon_0)^{1/2}\{\hat{a}_{kj}(t)\boldsymbol{\epsilon}(\mathbf{k}_+,j)T_{kj}\exp(i\mathbf{k}_+\cdot\mathbf{r})$$

$$+\hat{a}'_{kj}(t)[\boldsymbol{\epsilon}(\mathbf{k}_-,j)\exp(i\mathbf{k}_-\cdot\mathbf{r})+\boldsymbol{\epsilon}(\mathbf{k}_+,j)R'_{kj}\exp(i\mathbf{k}_+\cdot\mathbf{r})]\} \; ,$$
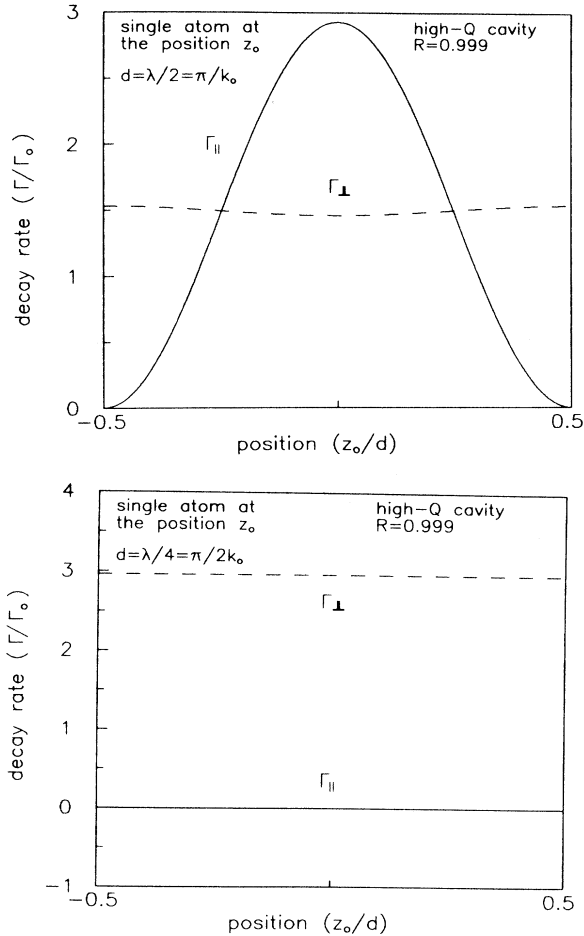
(5.1)

FIG. 2. Decay rates $\Gamma_\parallel(z_0)$ and $\Gamma_\perp(z_0)$ of a single dipole μ placed at position z_0 in a symmetrical microcavity, with orientation respectively parallel and orthogonal to the mirrors and in conditions of SpE "enhancement" (upper curve) and "inhibition" (lower curve) for a cavity confined by ideal mirrors with reflectivities ≈ 1 and independent of the incidence angle Θ. All quantities graphed in Figs. 2–4 are dimensionless.
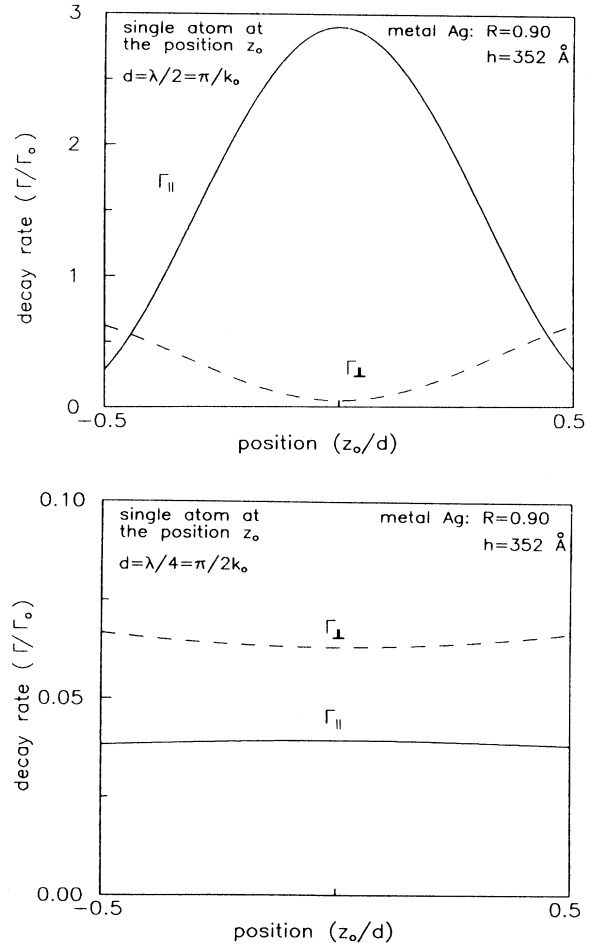
FIG. 3. Decay rates $\Gamma_\parallel(z_0)$ and $\Gamma_\perp(z_0)$ of a single dipole μ as for Fig. 2 but for a microcavity confined by two equal metal-Ag coated mirrors with normal-incidence reflectivity: $R(\Theta=0°)\equiv R=0.90$ at the SpE wavelength $\lambda=6111$ Å. In all figures the mirror reflectivity at $\Theta=0°$ is indicated by R and the calculated thickness of the coating h is expressed in angstroms (Å).

where **r** is assumed to have a positive z component and the time dependence of the field is carried by the Heisenberg destruction operators. Their time dependence is determined by Heisenberg's equation of motion with an interaction Hamiltonian given by (3.6). The solutions are found by the method given, for example, in Chap. 5.11 of Ref. 10 with appropriate generalization to allow for the more complicated spatial modes of the cavity. Thus the results for the driven parts of the field destruction operators are

$$\hat{a}_{\mathbf{k}j}(t) = -(ck/16\pi^3\epsilon_0\hbar)^{1/2}\int_0^t dt'\exp[ick(t'-t)][\epsilon(\mathbf{k}_+,j)t_{1j}^*\exp(-i\mathbf{k}_+\cdot\mathbf{r}_0)$$
$$+\epsilon(\mathbf{k}_-,j)t_{1j}^*r_{2j}^*\exp(-i\mathbf{k}_-\cdot\mathbf{r}_0-ikd\cos\Theta)]\cdot\hat{\Pi}(t')/D_j^* \tag{5.2}$$

and

$$\hat{a}_{\mathbf{k}j}'(t) = -(ck/16\pi^3\epsilon_0\hbar)^{1/2}\int_0^t dt'\exp[ick(t'-t)][\epsilon(\mathbf{k}_-,j)t_{2j}^*\exp(-i\mathbf{k}_-\cdot\mathbf{r}_0)$$
$$+\epsilon(\mathbf{k}_+,j)t_{2j}^*r_{1j}^*\exp(-i\mathbf{k}_+\cdot\mathbf{r}_0-ikd\cos\Theta)]\cdot\hat{\Pi}(t')/D_j^* \ , \tag{5.3}$$

where

$$\hat{\Pi}\equiv\mu|f\rangle\langle i| \tag{5.4}$$

is the projection operator that couples the atomic initial and final states involved in SpE. The electric vector of the emitted field is now obtained by substitution of (5.2) and (5.3) into (5.1). The resulting expression is quite complicated, but for the experiment reported in this paper it is sufficient to consider the observation points that have the same x and y coordinates as the radiating atom. Then if α and β are the polar angles of the atomic transition dipole moment μ, as shown in Fig. 1, so that

$$\mu=\mu(\sin\alpha\cos\beta,\sin\alpha\sin\beta,\cos\alpha) \ , \tag{5.5}$$

the x component of the field operator (5.1) obtained after some tedious algebra with the use of (2.1)–(2.3) and (2.8)–(2.11) is

$$\hat{E}_x^+(z,t) = -i(c\mu\sin\alpha\cos\beta/16\pi^2\epsilon_0)$$
$$\times\int_0^\infty dk\int_0^1 dC\int_0^t dt'\hat{\Pi}(t')k^3\exp[ick(t'-t)]$$
$$\times(t_{21}\{\exp[ikC(z-z_0)]+r_{11}\exp[ikC(z+z_0+d)]\}/D_1$$
$$+C^2t_{22}\{\exp[ikC(z-z_0)]+r_{12}\exp[ikC(z+z_0+d)]\}/D_2+\text{c.c.}) \quad (C\equiv\cos\Theta) \ , \tag{5.6}$$

where the azimuthal part of the wave-vector integral (3.4) has been performed. The two contributions to the field at position z correspond to direct propagation from the atom at position z_0 by transmission through the second mirror and indirect propagation in which the SpE light is reflected by the first mirror before transmission through the second mirror to give a total path length $(z+z_0+d)$. The effects of multiple reflections of the SpE light inside the cavity before it emerges to reach the observer at position z are included in the denominators D_j given by (2.8), which can be expanded as

$$D_j = \sum_{n=0}^\infty r_{1j}^n r_{2j}^n\exp(i2kCnd) \ . \tag{5.7}$$

Insertion of this expression into (5.6) produces a difficult angular integration since the r_{ij} and t_{ij} are functions of Θ. However, for observations that take place many wavelengths distant from the cavity, that is, for

$$kz\gg1 \ , \tag{5.8}$$

it is sufficient to make a dipole approximation and to retain only contributions of lowest order in $1/kz$. Then if the part of the integrand in small boldface parentheses in (5.6) is expanded in powers of $\sin^2\Theta$, except for the exponential factors, it is straightforward to show that only the terms of zeroth order in $\sin^2\Theta$ contribute to the far field in the lowest order of $1/kz$. Thus the reflection and transmission coefficients in (5.6) can be set equal to their constant polarization-independent $\Theta=0°$ values r_{i0} and t_{i0}, and the angular integration then gives the result

$$\hat{E}_x^+(z,t) = -(c\mu\sin\alpha\cos\beta/8\pi^2\epsilon_0)$$
$$\times\int_0^\infty dk\int_0^t dt'\hat{\Pi}(t')k^2\exp[ick(t'-t)]$$
$$\times\sum_{n=0}^\infty t_{20}r_{10}^n r_{20}^n\{\exp[ik(z-z_0+2nd)]/(z-z_0+2nd)$$
$$+r_{10}\exp[ik(z+z_0+d+2nd)]/(z+z_0+d+2nd)-\text{c.c.}\} \ . \tag{5.9}$$

The predominance of small values of Θ is of course physically reasonable for the situation considered here in which the line connecting the radiating atom to the distant observation point is perpendicular to the cavity mirrors. In order to perform the time integral, it is necessary to substitute a time dependence for $\Pi(t)$. The decay rate for an atom with dipole-moment orientation (5.5) is

$$\Gamma(z_0,\alpha) = \Gamma_\parallel(z_0)\sin^2\alpha + \Gamma_\perp(z_0)\cos^2\alpha \qquad (5.10)$$

and integration of this expression over α reproduces the result given in (4.17). The time dependence of the atomic operator is therefore[10]

$$\hat{\Pi}(t') = \hat{\Pi}(0)\exp[-ick_0t' - \tfrac{1}{2}\Gamma(z_0,\alpha)t'] \qquad (5.11)$$

to a sufficiently good approximation. The time integral in (5.9) then gives

$$\frac{-i\hat{\Pi}(0)\{\exp[-ick_0t -\tfrac{1}{2}\Gamma(z_0,\alpha)t]-\exp(-ickt)\}}{\{c(k-k_0)+i\tfrac{1}{2}\Gamma(z_0,\alpha)\}} . \qquad (5.12)$$

This expression has only a single simple pole in the lower half of the complex k plane. The final integral over k in (5.9) is performed by contour integration after extending its range to $-\infty$ in the usual way.[17] A careful consideration of the residues in the contour integration shows that the only nonzero contributions come from terms in the integrand of (5.9) where positive spatial imaginary exponentials multiply the second temporal exponential in (5.12) and the result is

$$\hat{E}_x^+(z,t) = -(k_0^2\mu\sin\alpha\cos\beta/4\pi\epsilon_0)$$

$$\times \sum_{n=0}^{\infty} t_{20}r_{10}^n r_{20}^n \{\hat{\Pi}[t-(z-z_0+2nd)/c]/(z-z_0+2nd)$$

$$+r_{10}\hat{\Pi}[t-(z+z_0+d+2nd)/c]/(z+z_0+d+2nd)\} , \qquad (5.13)$$

where the decay rate has been assumed: $\Gamma(z_0,\alpha) \ll ck_0$. The ordinary free-space source-field operator is recovered upon making the substitutions (4.9) when (5.13) reduces to[10]

$$\hat{E}_x^+(z,t) = -(k_0^2\mu\sin\alpha\cos\beta/4\pi\epsilon_0)$$

$$\times \hat{\Pi}[t-(z-z_0)/c]/(z-z_0) . \qquad (5.14)$$

The expression (5.13) clearly shows the contributions to the radiated field from the different numbers of reflections in the cavity mirrors, and the calculation demonstrates the straightforward application of the complete set of modes (2.6) and (2.7) for the cavity interior and exterior.

VI. EMISSION INTENSITY

The photocurrent produced by the radiated field in a detector placed at the observation point is proportional to the optical intensity or Poynting vector at coordinate z. Consider a situation in which the microcavity spacing is of the order of λ and the radiative decay time of the atom is very much longer than its period of oscillation. The differences between the retardation times in the various contributions to the radiated field (5.13) can then be ignored, and the form of the modulus of the Poynting vector appropriate to the rate of photodetection is then proportional to[10]

$$\langle \hat{E}^-(z,t)\cdot\hat{E}^+(z,t)\rangle$$

$$=K\sin^2\alpha\langle\hat{\Pi}^+(t-z/c)\cdot\hat{\Pi}(t-z/c)\rangle , \qquad (6.1)$$

where K is a constant obtainable from (5.13).[6] The atomic expectation value has a time dependence given by

$$\langle \hat{\Pi}^+(t)\cdot\hat{\Pi}(t)\rangle = \langle \hat{\Pi}^+(0)\cdot\hat{\Pi}(0)\rangle\exp[-\Gamma(z_0,\alpha)t] , \qquad (6.2)$$

where the decay rate is defined in (5.10). Suppose that a large number of randomly oriented atoms are simultaneously excited at coordinate z_0, at time $t=0$. The Poynting vector (6.1) then has a time dependence determined by the orientation-averaged function,

$$F(t) = \int_0^{(1/2)\pi} d\alpha \sin^3\alpha \exp\{-[\Gamma_\parallel(z_0)\sin^2\alpha + \Gamma_\perp(z_0)\cos^2\alpha]t\} . \qquad (6.3)$$

If the time is replaced by a new variable q defined as

$$q^2 = [\Gamma_\perp(z_0)-\Gamma_\parallel(z_0)]t , \qquad (6.4)$$

the integration in (6.3) can be performed in terms of the error function, $\text{erf}(q)$,[18] and the result is,

$$F(t) = \{\exp[-\Gamma_\parallel(z_0)t]/2q\}$$

$$\times[\pi^{1/2}(1-\tfrac{1}{2}q^{-2})\text{erf}(q)+\exp(-q^2)/q] . \qquad (6.5)$$

This result is valid for $\Gamma_\perp(z_0) > \Gamma_\parallel(z_0)$, i.e., when q is real. If $\Gamma_\perp(z_0) < \Gamma_\parallel(z_0)$ so that q is a pure imaginary, the result still holds except for the replacement:

$$\text{erf}(q) \to i\,\text{Im}\,\text{erf}(q) . \qquad (6.6)$$

The function $F(t)$ reverts to its expected exponential form when the spontaneous emission is isotropic, i.e., for $\Gamma_\parallel(z_0)=\Gamma_\perp(z_0)=\Gamma(z_0)$,

$$F(t) = \tfrac{2}{3}\exp[-\Gamma(z_0)t] . \qquad (6.7)$$

However, the decay of the atomic emission intensity otherwise shows nonexponential behavior. The general

short-time expansion of (6.5) is

$$F(t) = \tfrac{2}{3}\{1 - \tfrac{1}{5}[\Gamma_\perp(z_0) + 4\Gamma_\parallel(z_0)]t + O(t^2)\} \quad (6.8)$$

where the last term is of order t^2. It should be emphasized that the nonexponential form derived above is purely a consequence of the anisotropy of the atomic decay rate (5.10) with respect to the dipole orientation relative to the cavity axis. Markovian conditions are assumed for the Fermi golden rule calculation that leads to (6.5). In contrast to the above calculation there are of course well-known examples of nonexponential decay that occur as a result of non-Markovian effects.[19] Such effects predominate when the coherence time of the reservoir of field modes accessible to spontaneous emission becomes comparable to or longer than the characteristic time of the atom-field interaction. This regime is important to micromaser experiments (see Ref. 20 and earlier references therein).

VII. COMPUTER SIMULATION

A computer simulation of the above theory has been undertaken considering the relevant cases of a microcavity terminated by mirrors bearing metal coatings and dielectric-multilayered coatings. In the following discussion d represents the FP cavity spacing, i.e., the physical z dimension available for the active medium.

A. Metal mirrors

The numerical values of the real and imaginary parts of the dielectric constant of silver, the metal used in the experiment, $\epsilon = \epsilon' + i\epsilon'' = (n^2 - k^2) - i2nk$, at the wave length $\lambda \approx 6111$ Å are found as follows. For silver (Ag, evaporated) $n = 0.062$ $k = 3.85$, the maximum reflection is at $\Theta = 0°$ and $R_{max} = 0.985$.[9] The computer simulation has been carried out also for aluminum and a few results will be presented for this metal for comparison: $n = 1.10$, $k = 6.402$, $R_{max} = 0.91$ (Al,evaporated). Figure 3 shows the decay rates $\Gamma_\parallel(z_0) \equiv (T_\parallel)^{-1}$, $\Gamma_\perp(z_0) \equiv (T_\perp)^{-1}$ for a single atom placed at positions z_0 in a symmetrical cavity with $d = \bar{d} \equiv \tfrac{1}{2}\lambda$ and $d = \tfrac{1}{2}\bar{d}$, i.e., in the condition of "SpE enhancement" and "SpE inhibition," respectively.[3,4] These conditions are clearly represented by the corresponding behavior of $\Gamma_\parallel(z)$ and $\Gamma_\perp(z)$ as these quantities are proportional to the appropriate components of the vacuum-field energy density in the cavity. The $\cos^2(\pi z_0/d)$ dependence of the vacuum-field density is of course determined by the intracavity field-interference properties which, in turn, are determined by the FP boundary conditions.[9] The simulation shows that the condition of constructive interference, i.e., "SpE enhancement," is determined by a value of d which is resonantly peaked about $\bar{d}$ with a linewidth strongly determined by the cavity "finesse": $f = \pi R^{1/2}/(1-R)$, $R^2 = R_1 R_2$, with $R_1 \equiv |r_{10}|^2$ and $R_2 \equiv |r_{20}|^2$ being the mirror reflectivities at $\Theta = 0°$.[9,21] The "inhibition" corresponds instead to a far broader out-of-resonance behavior. All this is shown by Fig. 4, reporting, for a single atom placed at the center of a cavity bound by Ag and Al mirrors, the functional dependence of $\Gamma_\parallel(0)$ and $\Gamma_\perp(0)$ on

the cavity spacing d. Note the strong-inhibition plateau $\Gamma_\parallel/\Gamma_0 \ll 1$, for $d < \bar{d}$, i.e., the region sometimes referred to as the "optical Casimir effect," and the progressive trend, for increasing $d > \bar{d}$, toward the usual behavior of "macroscopic" cavities: $\Gamma_\parallel/\Gamma_0 = \Gamma_\perp/\Gamma_0 = 1$. Note, by comparison of the two plots for silver and aluminum in Fig. 4 which correspond to the *same* mirror R values, the effect of the different metal absorption on the behavior of $\Gamma_\parallel$ and $\Gamma_\perp$. On the basis of the single-atom results, the overall many-atom SpE radiation detected outside the cavity on a single spatial mode with **k** vector parallel to the cavity axis could be determined. Figures 5 and 6 show, for Ag mirrors with $R = 0.90$, two SpE pulses for "enhancement" and "inhibition" conditions, due to the contribution of all atoms completely filling the cavity, i.e., placed at different z positions and for isotropic orientation of μ. These curves, as well as the ones of Fig. 8, are obtained by integration of (6.5) over z_0 for the two significant values of d: $d = \bar{d}$, $d = \tfrac{1}{2}\bar{d}$. In the simulation the integral has been carried out by assuming a decompo-
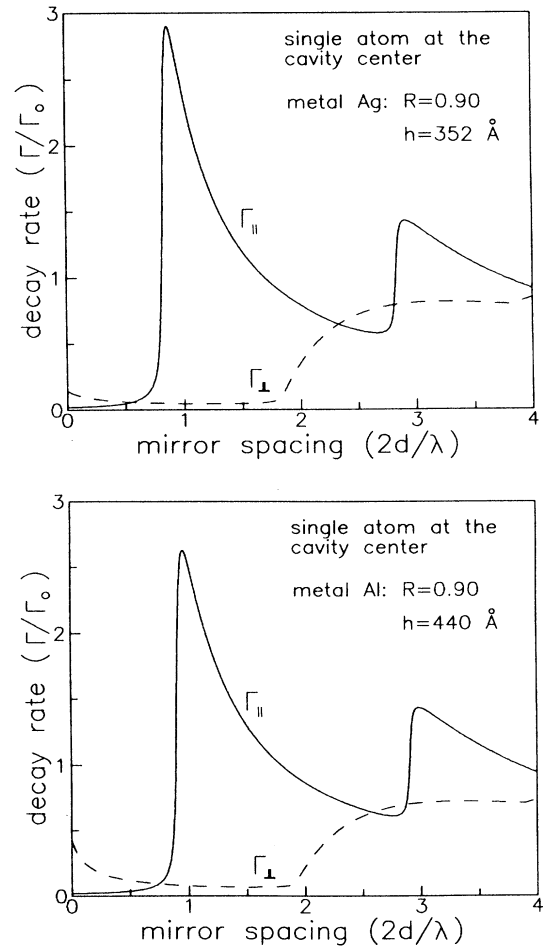

FIG. 4. Decay rates of a single dipole placed at the center, $z_0 = 0$, of a symmetrical microcavity terminated by two real, equal mirrors as functions of the cavity spacing and for Ag and Al coatings with equal R (0°) = 0.90, $\lambda = 6111$ Å.

sition of the cavity volume in 500 plane layers for each fraction $\Delta d = \frac{1}{2}\lambda$ of the cavity spacing and then by summing the respective contributions at the detector, neglecting retardation. Note the nonexponential behavior in Figs. 5 and 6 due to the process previously discussed in Sec. 6. Owing to this effect we may define an overall "relaxation time" T as the time at which the nonexponential detected pulse reaches a value equal to e^{-1} of the maximum. The d dependence of T relative to the free-space value $T_0 \equiv (\Gamma_0)^{-1}$ is reported by the two curves given in Fig. 7, with two different scales, for an isotropic active medium completely filling a symmetrical microcavity terminated by Ag mirrors bearing respectively the maximum attainable value of R, $R_{max} = 0.985$, and the value $R = 0.90$ adopted in the experiment. The curves of Fig. 7 express the result of a very lengthy numerical computation of a large number of values of T/T_0, each one ob-
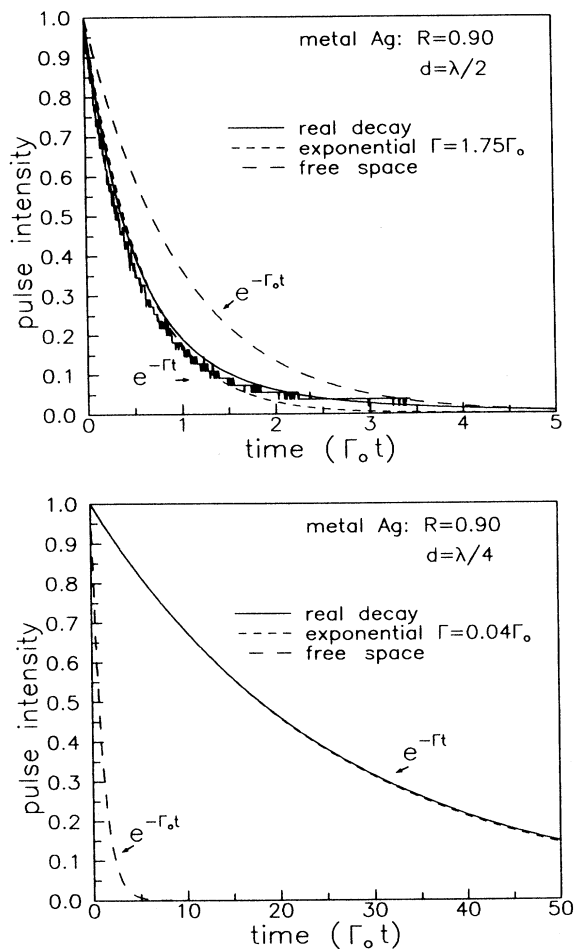

FIG. 6. SpE pulse (arbitrary units) corresponding to the one of Fig. 5 for the "enhancement" condition and drawn in semilogarithmic scale. The experimental result, the same as Fig. 5, upper curve, demonstrates the nonexponential decay.

FIG. 5. SpE pulse (arbitrary units) detected outside a symmetrical microcavity terminated by Ag coatings, $R(0°) = 0.90$ and filled with randomly oriented active-dipoles in conditions of SpE enhancement and inhibition. In the upper graph the experimental decay curve for SpE enhancement is also shown. In inhibition condition the "real" and the exponential decay curves nearly overlap. As for Figs. 6 and 8, the curves are plotted as functions of the dimensionless "time" $(\Gamma_0 t)$.
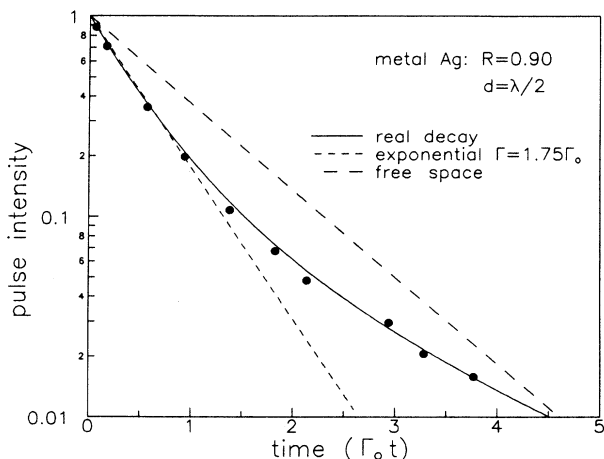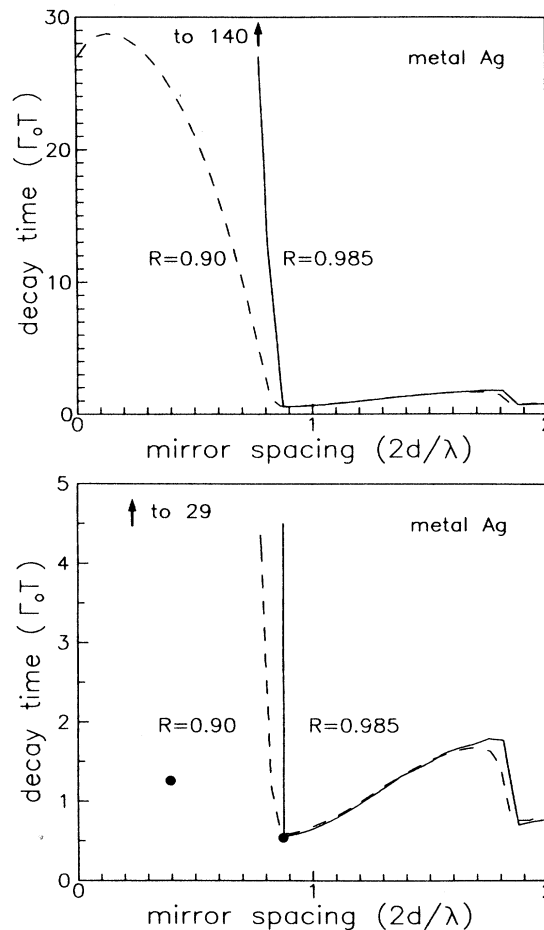

FIG. 7. SpE-signal decay time computed as a function of the (dimensionless) spacing of a symmetrical microcavity filled with randomly oriented active dipoles for confinement due to Ag mirrors with $R(0°) \approx R_{max} = 0.985$ and $R(°) = 0.90$ at $\lambda = 6111$ Å. The two graphs are presented with two different scales and report the two maximum values of $(\Gamma_0 T)$ attainable, respectively, with $R = 0.985$ and 0.90. The two dots on the lower graph represent the results of Fig. 11.

tained for different d by integration over z_0. The results for R_{max} in Fig. 7 may be taken to establish the theoretical limit performance of the microcavity terminated by metal mirrors with respect to realization of the "anomalous" behavior in SpE. An important conclusion may be drawn by a close examination of the results of all computations and of Figs. 2–8, just discussed. It appears there, and very clearly in Figs. 2, 3, 4, and 7, that the condition of "SpE enhancement" is generally weakly affected by substantial changes of the physical parameters of the microcavity, as for instance by the values of the mirror reflectivities, or by the presence of interatom superradiant couplings, or even by making the simplifying assumption of Θ independent of r_{1j}.[8] On the other hand, the inhibition condition appears to be strongly affected by all optical parameter perturbations and seems then critically dependent on all physical conditions affecting the active microcavity. This somewhat "unstable" behavior, characteristic of SpE inhibition, appears to be rooted in the spontaneous-emission process itself as it shows up in all computational results. In addition to that and most important, it also shows up in all experimental observa-

tions and measurements, as demonstrated by the experimental data reported in Fig. 7.

B. Semiconductor-multilayered mirrors

The spontaneous-emission theory given in the previous sections is assumed approximately valid for a microscopic cavity bound by mirrors bearing thick, dielectric-multilayered coatings. The idea behind this assumption is that, in spite of the thickness of the coatings, the excited atoms in the process of SpE actually are influenced by the multilayered-dielectric stacks providing vacuum confinement only through their overall, "external" optical parameters. In this connection, the first task to fulfill within a computer simulation consists of the calculation of these external parameters by adopting a reliable computational algorithm to solve simultaneously the large number of boundary-condition equations involved in the problem. Before doing that in order to start the SpE-microcavity simulation, we felt it nevertheless necessary to test first experimentally the validity of the algorithm used by checking the correspondence between the results of a computer calculation, based on that algorithm, of the external optical parameters of any real multilayered mirror and the corresponding values of these parameters measured with the same mirror. The results of this side experiment, described in the Appendix, have been found to test satisfactorily the algorithm by Lissberger and Wilcock.[22] Therefore this algorithm has been chosen as the computational basis of the main microcavity simulation. The structure of the coatings, equal for the two cavity mirrors, deposited over circular, plane fused silica substrates with planarity $\lambda/20$ over the diameter ($=25.4$ mm), consisted of 23 alternate, unequal thickness h' layers made by two dielectric materials with different refractive indices n at the SpE wavelength $\lambda=6111$ Å. The sequence of h' values given in units of 10^{-2} μm was as follows:[23,24] (Substrate $|L\ 4.83|H\ 8.17|L\ 9.67|H\ 8.17|L\ 8.17|L\ 10|H\ 8.17|L\ 9.67|H\ 8.17|L\ 9.67|H\ 8.17|L\ 9.67|H\ 8.35|L\ 9.86|H\ 8.35|L\ 9.86|H\ 8.35|L\ 9.86|H\ 8.35|L\ 9.86|H\ 8.35|L\ 9.86|H\ 8.35|L\ 4.93|$ air). There the L label represents the material ThF$_4$, $n=1.514$, while H represents Sb$_2$O$_3$, $n=2.01$. The spectrophotometric trace of the mirrors showed a wide reflectivity peak with $R\ (\Theta=0°)\approx0.98$, centered at $\lambda\approx6000$ Å and with bandwidth approximately equal to 800 Å. The transmittivity at the excitation wavelength, $\lambda_p\approx3547$ Å, was $T(0°)\approx0.85$. SpE results similar to the ones obtained for the metal coatings, Figs. 3–7, were obtained for the multilayered mirrors. We only show in Fig. 8 the SpE nonexponential decaying pulses for enhancement and inhibition conditions. They are obtained, as are the results reported in Fig. 5, by integrating (6.5) over z_0 for $d=\bar{d}$ and $d=\frac{1}{2}\bar{d}$. We notice, by comparison of Figs. 5 and 8, that the effect of vacuum confinement may be comparable and even larger for metal mirrors in spite of the cavity damping due to optical absorption. In fact, the favorable condition due to the virtual absence of absorption of the dielectric coatings is generally counterbalanced by their higher reflectivity losses at large Θ, as discussed at length in the Appendix. However, this negative effect may in turn be
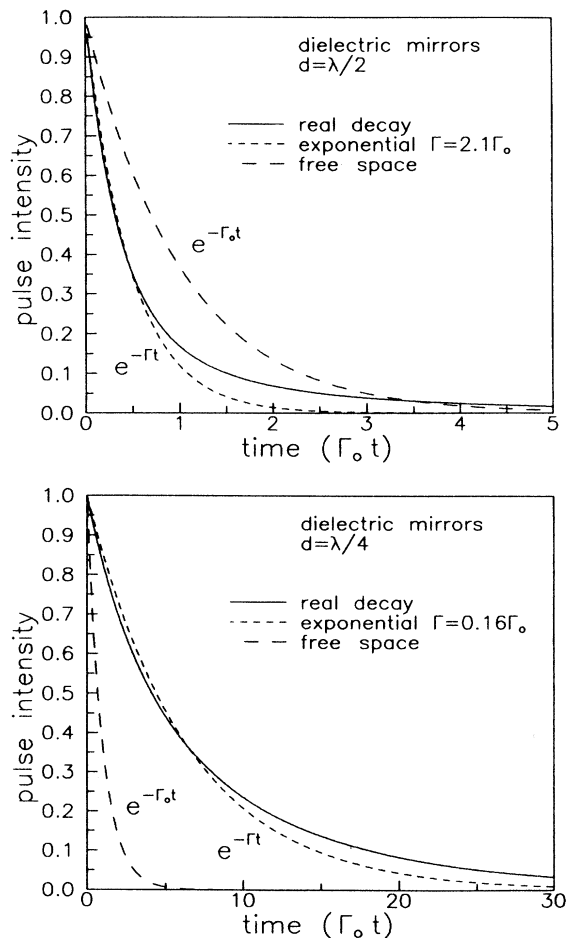
FIG. 8. SpE pulse detected outside a symmetrical microcavity terminated by the dielectric-multilayered coated mirrors used in the experiment (see text).

compensated for by adopting a wide enough reflectivity band of these coatings.[24]

VIII. EXPERIMENTAL RESULTS

The piezoelectrically [piezoelectric transducer (PZT)] tuned Fabry-Pérot microcavity adopted in our experiment was composed of two plane metal-coated or multilayered-coated mirrors, labeled by A and B in Fig. 9, with diameter 25.4 mm and planarity $\geq \lambda/20$. Several mirror combinations were adopted. For instance, with A highly reflecting the SpE radiation (with wavelength λ) and highly transmitting the "pump" radiation (with wavelength λ_p), and B highly reflecting both wavelengths, the excitation method of "periodic pumping" could be adopted.[4,25] The value of the overall cavity "finesse," typically $f \approx 20$–30, was determined as usual by measuring the relative widths of the resonant peaks of the transmission function obtained by piezoelectrically tuning the microcavity spacing. In this case the resonator was excited at normal incidence, $\Theta = 0°$, by a parallel Gaussian He-Ne laser beam with a full-width diameter ≈ 10 mm.[8,26] The cavity spacing d was tuned by means of the large toroidal piezoelectric transducer shown in Fig. 9. In all experiments involving fluorescence detection at $\lambda = 6328$ Å, the absolute value of d was obtained by simple determination of the FP interference patterns on a screen under excitation by a He-Ne laser. For SpE detection of wavelengths other than $\lambda = 6328$ Å, the absolute value of d was determined by setting at the appropriate value, calculated by interpolations based on values suitable for $\lambda = 6328$ μm, the voltage applied to the cavity-tuning piezoelectric transducer. Several types of active media were used in our SpE experiments. We have reconfirmed the early experimental results reported by De Martini and Innocenti in Fig. 2 or Ref. 4, with rhodamine dyes having free-space SpE lifetimes, $T_0 = 5$–15

nsec. Precisely, we have successfully tried rubrene (solvent: ethyl alcohol), sulforhodamine 640 (ethyl alcohol), DCM (ethyl alcohol, ethylene glycol, gylcerol). In all cases the dye concentration was 10^{-4}–$10^{-3}M$. Two different excitation or detection methods were adopted. By a first technique, already described in Refs. 4 and 5, the dye was excited by 2 nsec, $\lambda_p = 5320$ Å, second-harmonic generation (SHG) laser pulses using as primary source an unstable-cavity self-injected neodymium-doped yttrium-aluminum-garnet (Nd:YAG) laser.[27] The shape of the SpE single pulses was detected along the cavity axis by a high quantum-efficiency Quantacon photomultiplier RCA C31034A-02 and then registered by a 1.3-Ghz bandwidth Le-Croy 8013A waveform digitizer. By a second technique, the dye was excited by picosecond, $\lambda_p = 5320$ Å pulses generated by a Coherent-Antares mode-locked laser and the average SpE pulse shape was determined by a single-photon-counting technique via a time-to-height-converter device.[28] Both methods gave comparable, satisfactory results. However, in the present work we wanted to study spontaneous-emission effects from an active medium that could present a spectroscopic structure simpler and more transparent than for the broadband molecular dyes used before. This should allow the investigation of a definite atomic level having a narrow enough inhomogeneous-broadening linewidth, $\Delta v = (T_2^*)^{-1}$, and a large free-space SpE time T_0.[29,30] We have investigated in detail SpE from europium atoms in dibenzoylmethane $(DBM)_4$ complex that shows sharp emission lines about $\lambda \approx 6000$ Å. For this complex we have determined experimentally the fluorescence curve at room temperature under uv excitation, $\lambda_p = 3547$ Å. Figure 10 shows that at least three emission lines of the Eu-atom ^5D-^7F multiplet can be clearly identified at room temperature. We have investigated experimentally the strongest line, $^5D_0$-$^7F_2$ at $\lambda = 6111$ Å, for which the free-space SpE time has been found: $T_0 \approx 560$ μsec for
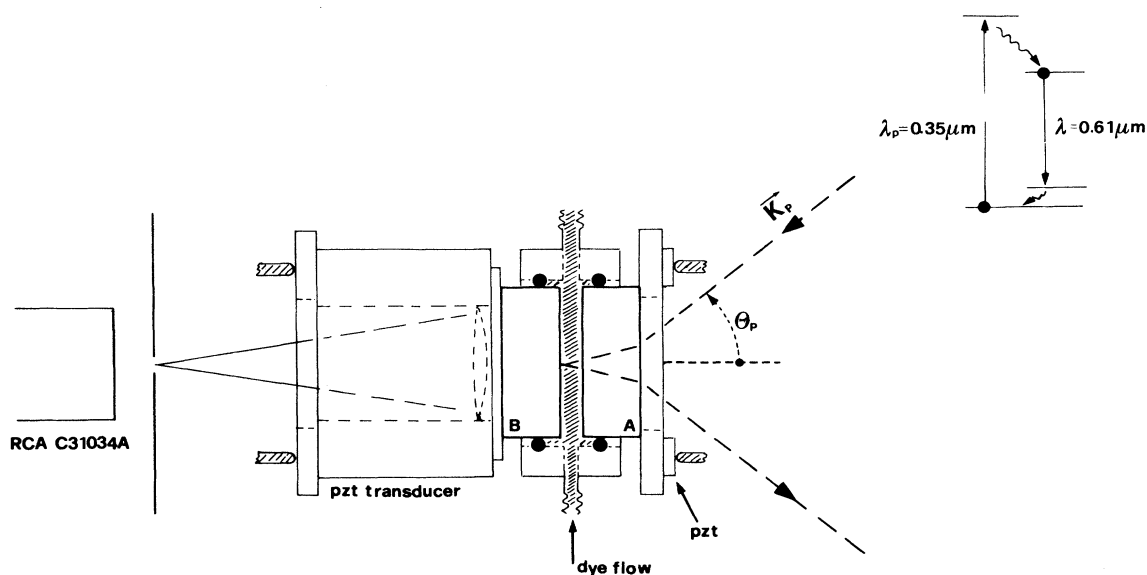

FIG. 9. Piezoelectrically (PZT) tuned Fabry-Pérot microcavity (section). The adjustment of the direction angle Θ_p of the incoming pump K_p vector allows the realization of the "periodic-pumping" technique; cf. Ref. 25.

ethylene-glycol solution at a temperature of 300 K and $T_2^* \approx 400$ fsec. The excitation was provided by a well-collimated TEM_{00}-mode coherent beam at $\lambda_p = 3547$ Å, third-harmonic generated by an unstable-cavity Nd:YAG laser with 5-nsec pulse duration and operating at 20 Hz. The excitation Gaussian beam, with a diameter of ≈ 8 mm, was injected near orthogonally to the cavity mirrors. The SpE pulses were detected through a $\Delta\lambda = 21$ Å full width at half maximum (FWHM) bandwidth interference filter by means of the same RCA Quantacon photomultiplier of the previous experiment, cooled down to -30 C°. The excitation energy was taken at a level so low that the average detected photoelectrons per pulse were $\approx 10-20$. The SpE pulses were reconstructed by averaging over 2×10^3 pulses by a Le-Croy 9400 digital oscilloscope.

Figures 11 and 13 show the SpE decay of Eu-$(DBM)_4$ complex in a symmetrical microcavity terminated respectively by Ag mirrors and by dielectric-multilayered mirrors in SpE enhancement, $d = \bar{d}$, and inhibition, $d \approx \frac{1}{2}\bar{d}$, conditions at a pump pulse energy $\approx 10^{-7}$ J. A sizable effect of time shortening due to merging of SpE into the regimes of StE and of thresholdless cooperative superradiance is shown in Fig. 12 for the inhibition condition, the one that appears to be mostly affected by all physical perturbations, as discussed at length in Sec. VII.[5,31] According to the result shown in Fig. 12 we may conclude that strictly speaking, in the SpE-inhibition condition, the regime of spontaneous emission is realized only asymptotically for excitation pulse energies decreasing toward zero. In this sense the experimental values of T/T_0

reported for SpE inhibition in Figs. 7, 11, 12, and 13 may be interpreted as lower-limit values rather than definite (i.e., asymptotic) values of the SpE decay time.

In summary, with our system we have verified experimentally the most relevant microcavity effects anticipated by the quantum theory of spontaneous emission. In particular, a good correspondence between the results of theory and experiment has been obtained for the effects related to the condition of SpE enhancement, namely, the value of the relaxation time T and the nonexponential shape of the detected pulse. The process of Spe inhibition has also been verified with our Eu-complex system. However, some comments should be devoted to the reasons that could have determined the small value of T detected with all kinds of mirror coatings. We do believe that these reasons are mostly of instrumental or experimental nature, in particular, related to the existence on any mirror surface of largely unavoidable microscopic irregularities having a size of about 10–100 Å. These surface irregularities, which have also been investigated in the experiment by means of a contact profilometer (Tencor-1), introduce localized perturbations of radiation confinement at the site of the single atoms that may be highly effective in impairing the inhibition process. On the other hand, the critical sensitivity of this process to all kinds of confinement perturbations, already discussed in Sec. VII, is not difficult to understand in simple terms. In fact, any externally and macroscopically induced inhibition of a quantum-decay phenomenon leads quite naturally to apparently "enhance" beyond the expected limits the effect
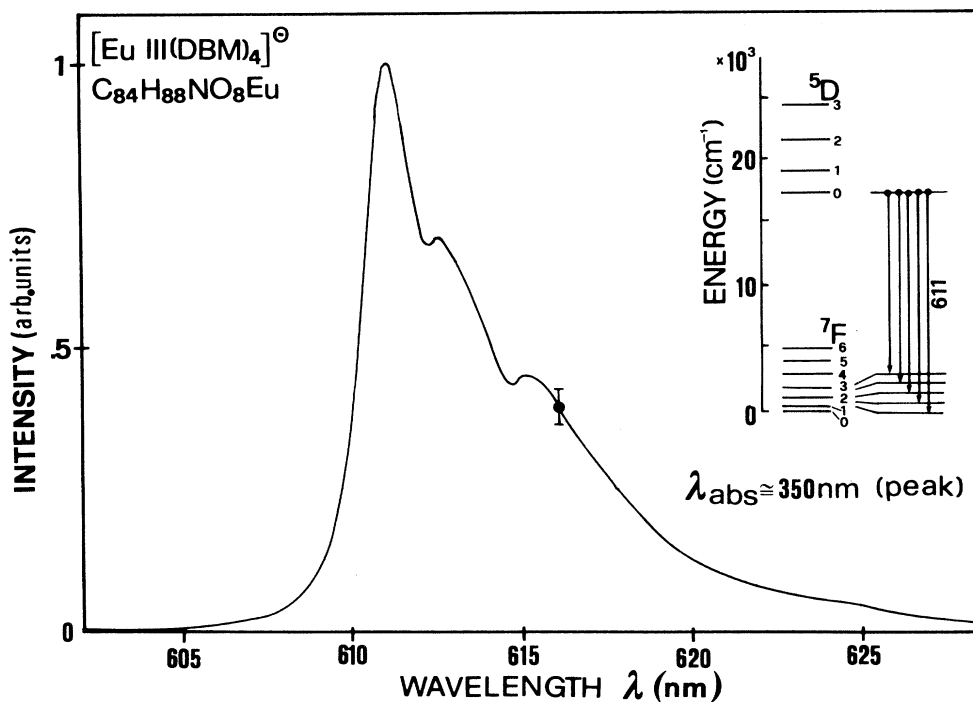

FIG. 10. Fluorescence curve, experimentally obtained, of Eu-dibenzoylmethane complex [Eu-$(DBM)_4$] under uv excitation at $\lambda_p = 3547$ Å at room temperature.
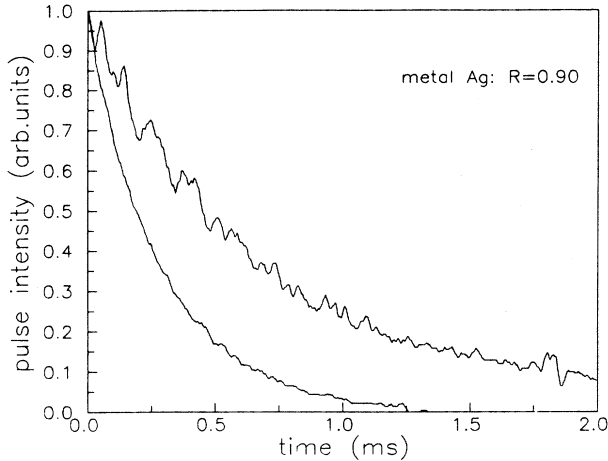
FIG. 11. Spontaneous-emission decay curves obtained with a symmetrical microcavity terminated by Ag-coated mirrors with $R=0.90$, in condition of "enhancement" ($d=\bar{d}\equiv\frac{1}{2}\lambda$, faster decay) and "inhibition" ($d\approx\frac{1}{2}\bar{d}$, slower decay). Active medium: Eu-$(DBM)_4$. The corresponding decay curve for SpE in "free space" (i.e., in the absence of cavity mirrors), with SpE time $T_0\approx560$ μsec, is reported in Fig. 13, curve (b). The curves here and in Fig. 13 are drawn by a computer average of 2×10^3 pulses registered at the photomultiplier output.

of all other deexcitation channels, on the microscopic and submicroscopic scale. By the same argument, any unavoidable small experimental error or imperfection, for instance of FP alignment, can play an unusually large role. In addition, the radiation leakage in the microcavity radial directions may be highly effective in reducing the confinement.[24] A few other important and fundamental effects may also impair the effect of SpE inhibition. We list them briefly.

(a) The transition at $\lambda=6111$ Å investigated in the SpE experiment is but one of the transitions of the ^5D-^7F multiplet that may provide alternative routes of deexcitation, larger wavelengths, of the $^5D_0$ level of Eu-$(DBM)_4$, as shown in Fig. 10.
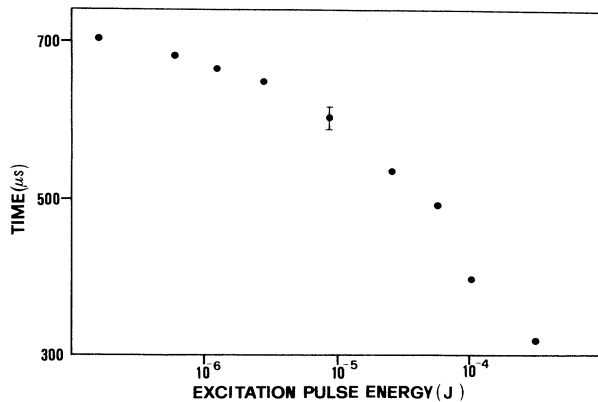
(b) The theory presented in this work assumes a

FIG. 12. SpE time as a function of the energy (joules) of the exciting pulse in the "inhibition" condition, obtained in the experiment leading to the results of Fig. 11. FWHM transverse section of the Gaussian pump beam: 8 mm.
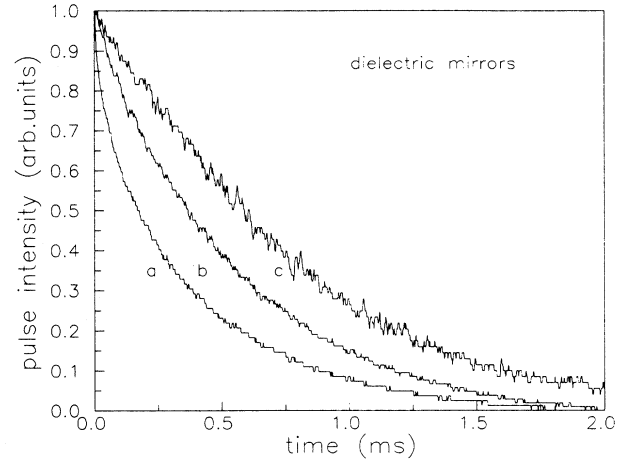

FIG. 13. Spontaneous-emission decay curves obtained with a symmetrical microcavity terminated by semiconductor-multilayered mirrors (cf. text). Curves (a) and (c) correspond to "SpE enhancement" ($d\approx\frac{1}{2}\bar{d}$) and "SpE inhibition" ($d\approx\frac{1}{4}\bar{d}$), respectively. Curve ($b$) represents SpE in "free space," with $T_0\approx560$ μsec. Active medium: Eu-$(DBM)_4$. The curves are drawn by a computer average of 2×10^3 pulses, as for Fig. 11.

linewidth of the emitting atom that is at most determined by the fluorescence time itself. On the other hand, the size of the experimental width of the $\lambda=6111$ Å fluorescence line of the Eu complex investigated in the experiment is only ten times narrower than the cavity linewidth determined by the microcavity finesse.[9]

(c) The theory presented in this work does not account for the processes of radiationless energy transfer between organic molecules and the mirror surfaces (See Drexhage[30] and Kuhn and Möbius[32] and Kuhn[32]). Since these processes are found to be important over distances from surfaces of the order of 500 Å, they should be effective in microcavities in the inhibition condition, i.e., for $d<\frac{1}{2}\lambda$.

IX. CONCLUSIONS

The main theoretical results of the paper are the expressions (4.4) and (4.8) for the SpE decay rates of atoms whose active dipole moments are oriented, respectively, parallel and perpendicular to the microcavity mirrors. These general results include a range of special cases, and there is agreement with previous work in appropriate limits. The theory is based on the complete set of modes described by (2.6) and (2.7). We believe that these modes provide a more convenient and reliable basis for all manner of radiative field calculations than do the discrete sets of modes that are sometimes constructed by artifically limiting infinite space by means of an enveloping fictitious "supercavity" of large but finite dimensions. Our method also straightforwardly produces the source-field operator given by (5.13) for the detection outside of the cavity of the radiative E field spontaneously emitted by an atom inside the cavity. Previous work in this field has been restricted to one-dimensional calculations that cannot adequately represent the spatial distribution of the spontaneous emission (Feng and Ujihara[33]). A

comprehensive computer simulation of the process of spontaneous emission is presented and leads to the calculations of all optical parameters investigated by the theory in the perspective of a comparison with the corresponding experimental results. The basic algorithm adopted in the computer calculation of all external optical parameters of the semiconductor multilayered structures is also tested experimentally. Then an experiment is presented aimed at the verification of the relevant theoretical results, namely the effects of spontaneous-emission enhancement and inhibition and of nonexponential shape of the detected SpE signals. All these effects are verified experimentally by the investigation of the spontaneous emission from the $^5D_0$-$^7F_2$ line of an Eu-$(DBM)_4$ complex adopted as the active medium and by the use of a microscopic cavity terminated by mirrors bearing either metal and dielectric coatings. A final discussion of the results is mainly devoted to the identification of the physical processes that may account for the somewhat reduced effect of SpE inhibition found in the experiment.

ACKNOWLEDGMENTS

APPENDIX: EXPERIMENTAL TEST OF A COMPUTER DETERMINATION OF THE EXTERNAL OPTICAL PARAMETERS OF A SEMICONDUCTOR LAYERED STRUCTURE

The adoption of the Lissberger-Wilcock algorithm[22] within our computer simulation is justified here by a detailed experimental check of the calculated values of the relevant external optical parameters of one particular multilayered-coated test mirror. The test mirror was one of the mirrors (mirror A) used in our original microcavity experiment.[4] The structure of the coating, deposited over a circular plane BK7 glass substrate with diameter $d=25.4$ mm and planarity $\lambda/20$, consisted of 28 alternate, unequal thickness h' layers made by two semiconductor materials with different refractive indices, n. The sequence of the h' values, given in units of 10^{-1} μm, was as follows:[23] (glass $|L$ 1.2$|H$ 5.3$|L$ 8.2$|H$ 5.3$|L$ 8.2$|H$ 5.5$|L$ 8.5$|H$ 5.5$|L$ 8.5$|H$ 5.8$|L$ 8.9$|H$ 5.8$|L$ 8.9$|H$ 6.0$|L$ 9.2$|H$ 6.0$|L$ 9.2$|H$ 6.2$|L$ 9.6$|H$ 6.2$|L$ 9.6$|H$ 6.4$|L$ 9.9$|H$ 6.6$|L$ 10.2$|H$ 6.6$|$ Air). The label L represents ThF$_4$, $n=1.51$ (at $\lambda=6328$ Å) while H represents ZnS, $n=2.45$ at the same λ. Figure 14 shows the good correspondence existing between the experimental spectrophotometric plot of the wavelength dependence of the mirror transmission coefficient $T(\lambda)\equiv|t|^2$ at normal incidence, $\Theta=0°$, and the related computer results. The Θ dependence of the reflectivity, $R(\Theta)\equiv|r|^2$ at $\lambda=6328$ Å has
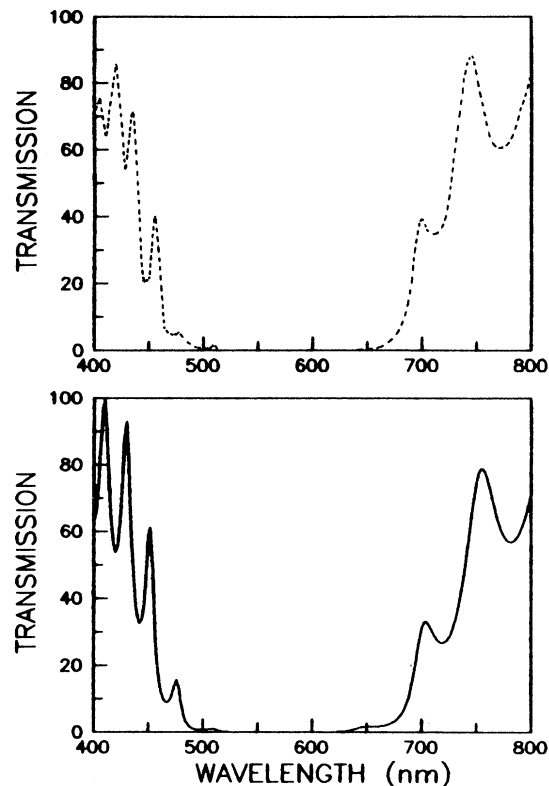

FIG. 14. Spectrophotometric trace of $T(\lambda)$, the transmittivity of the dielectric-multilayered coated test mirror at normal incidence, $\Theta=0°$ (upper trace). Corresponding result of computer calculation: (lower trace).

been determined for $\Theta < 70°$ by direct intensity measurements on a reflected single-mode He-Ne laser beam, for s and p polarizations. Figure 15 shows again a good correspondence with the computer calculated $R(\Theta)$. Note that the degree of vacuum confinement is reduced at large Θ, mainly for p polarization, owing to the typical
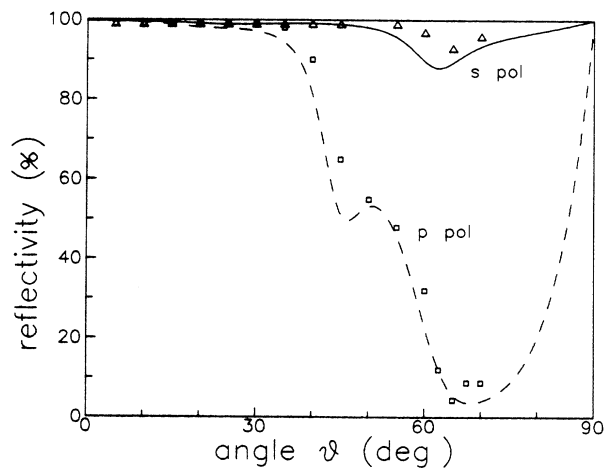

FIG. 15. Experimental and computer-calculated reflectivity $R(\Theta)$ at $\lambda=6328$ Å of the dielectric-coated test-mirror as a function of the incidence angle Θ.
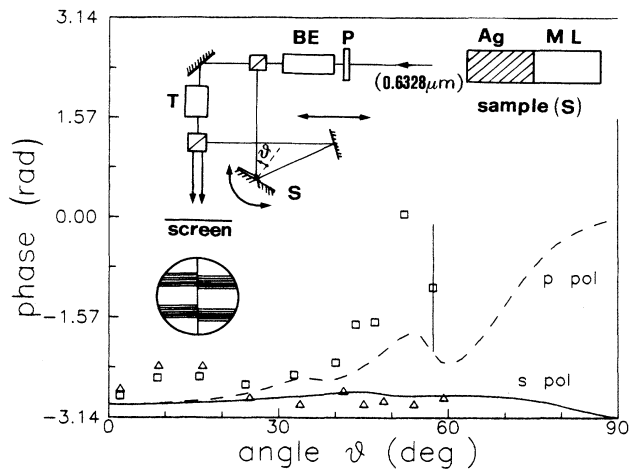
FIG. 16. Experimental and computer-calculated phase $\phi(\Theta)$ of the reflection coefficient of the dielectric-multilayered coated test mirror at $\lambda = 6328$ Å. The Mach-Zehnder interferometer adopted in the phase-test experiment is shown in the inset: P is a polarizer, BE a beam expander, T a telescope, and the half-silvered semiconductor-multilayered mirror is shown at the rhs.

angular dispersive effect of any layered structure.[24] Owing to this effect, the vacuum confinement is in general somewhat inhibited by the use of narrow-band mirrors, i.e., having a fully *periodic* layered coating structure (as for the reverse case of the interference filter). However, we have found that an increasingly larger confinement can be achieved up to a very high degree by the use of increasingly broader reflectivity bands. The virtual absence of damping in multilayered-electric coatings, as for instance with multiple-quantum well type structures, makes them most attractive in physical and technological applications involving microcavity SpE and StE processes, e.g., in thresholdless-laser applications.[4,5] In fact, the experiment reported by this work, with use of mirrors that are not especially broadband or made *ad hoc*, shows that a multilayered-dielectric confinement may lead to SpE results that are comparable to the ones corresponding to metal coatings in spite of the $R(\Theta)$ confinement limitations shown in Fig. 15. The information regarding the relevant optical parameters of the test mirror is completed by measurement and calculation of the phase $\phi(\Theta)$ of the complex reflection coefficient: $r(\Theta)$ $= [R(\Theta)]^{1/2} \exp \phi(\Theta)$. The inset in Fig. 16 shows the layout of the Mach-Zehnder interferometer built for this purpose. Half of the rectangular surface of a replica mirror, i.e., bearing a multilayered coating identical to the one of the test mirror, was additionally coated by an $h = 2000$ Å layer of evaporated Ag metal. The two interfering beams were obtained by reflecting two complementary portions of the Gaussian transverse section of a
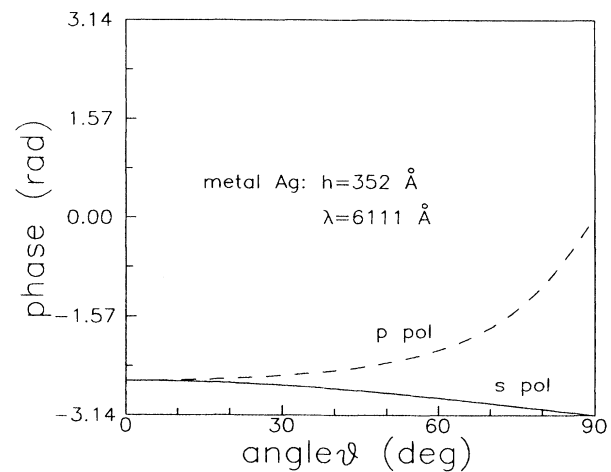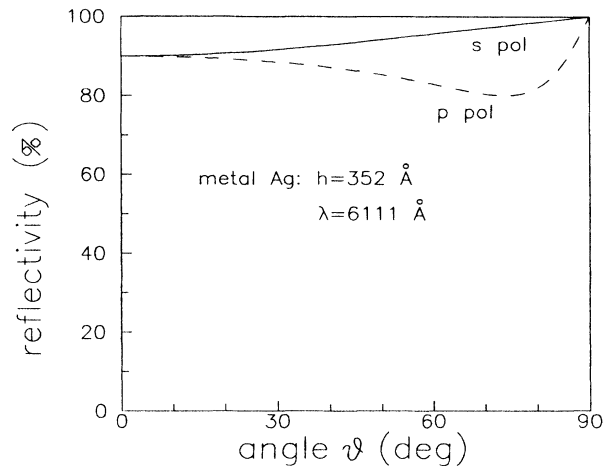
single TEM$_{00}$ He-Ne laser beam, after beam expansion to ≈ 8 mm diameter, by the two parts of the replica mirror bearing different coatings. The phase $\phi(\Theta)$ due to the reflection by the layered coating was determined, for s and p polarizations, by subtracting, from the overall $\phi_t(\Theta)$ phase measured by interference-fringe position, the phase contribution $\phi_m(\Theta)$ due to metal-coating reflection, whose computer calculation is standard.[9] The resulting $\phi(\Theta)$ values are given in Fig. 16, for s and p polarizations, with the corresponding results of the calculations based on Ref. 22. For the sake of completeness, the results of standard computer calculations of $R(\Theta)$ and $\phi_m(\Theta)$ for metal-Ag coating, $R = 0.90$, and for s and p polarizations are also given in Fig. 17.

FIG. 17. Calculated reflectivity $R(\Theta)$ and phase $\phi(\Theta)$ for an Ag-coated mirror with $R(0°) = 0.90$ at $\lambda = 6111$ Å, for s and p polarizations.

[1] E. M. Purcell, Phys. Rev. **69**, 681 (1946).
[2] C. H. Townes and A. Schawlow, *Microwave Spectroscopy* (McGraw-Hill, New York, 1955), p. 336; J. R. Ackerhalt, P. L. Knight, and J. H. Eberly, Phys. Rev. Lett. **30**, 456 (1973);

J. Ackerhalt and J. H. Eberly, Phys. Rev. D **10**, 3350 (1974); I. R. Senitzky, Phys. Rev. Lett. **31**, 955 (1973); P. W. Milonni, J. R. Ackerhalt, and W. A. Smith, *ibid.* **31**, 958 (1973); D. Kleppner, *ibid.* **47**, 233 (1981); J. Dalibard, J. Dupont-Roc,

and C. Cohen Tannoudij, J. Phys. **43**, 1617 (1982); E. T. Jaynes, in *Coherence and Quantum Optics,* edited by L. Mandel and E. Wolf (Plenum, New York, 1978); L. Allen and J. H. Eberly, *Optical Resonance and Two-Level Atoms* (Dover, New York, 1975), Chap. 7.

[3]P. Goy, J. Raymond, M. Gross, and S. Haroche, Phys. Rev. Lett. **50**, 1903 (1983); R. G. Hulet, E. S. Hilfer, and D. Kleppner, *ibid.* **55**, 2137 (1985); D. Meschede, H. Walther, and G. Muller, *ibid.* **54**, 551 (1985). For a review on SpE effects with Rydberg atoms, see P. Filipowicz, P. Meystre, G. Rempe, and H. Walther, Opt. Acta **32**, 1105 (1985). G. Gabrielse and H. Dehmelt, Phys. Rev. Lett. **55**, 67 (1985); W. Jhe, A. Anderson, E. A. Hinds, D. Meschede, L. Moi, and S. Haroche, *ibid.* **58**, 666 (1987), reported SpE microcavity work in the near infrared ($\lambda = 3.49$ μm) with a cw technique; D. J. Heinzen, J. J. Childs, J. E. Thomas, and M. S. Feld, Phys. Rev. Lett. **58**, 1320 (1987).

[4]F. De Martini and G. Innocenti, in *Quantum Optics IV,* edited by J. Harvey and F. Walls (Springer, Berlin, 1986). This work reports a proposal and realization of the microcavity and its application to spontaneous emission (SpE). Microcavity SpE studies have also been reported by F. De Martini and G. Innocenti, International Quantum Electronics Conference (IQEC) Tech. Digest XIV, 147 (1986), F. DeMartini, G. Innocenti, and P. Mataloni, IQEC Tech. Digest XV, 128 (1987); F. De Martini, G. Innocenti, G. Jacobovitz, and P. Mataloni, Phys. Rev. Lett. **59**, 2955 (1987).

[5]F. De Martini and G. R. Jacobovitz, Phys. Rev. Lett. **60**, 1711 (1988). F. De Martini, Phys. Scr. **21**, 58 (1988). Casimir-type *extreme* confinement is realized for quantum-field confinement over a space-time length $\approx \lambda_D$, the de Broglie wavelength of the corresponding particle. Examples are the microcavity, all kinds of particle diffraction, electrons in multiple-quantum-well structures.

[6]F. De Martini, M. Marrocco, and D. Murra, Phys. Rev. Lett. **65**, 1853 (1990); in *Coherence and Quantum Optics,* edited by J. H. Eberly and L. Mandel (Plenum, New York, 1990); F. De Martini, in *New Frontiers in QED and Quantum-Optics,* edited by A. Barut (Plenum, New York, 1990).

[7]M. Ley and R. Loudon, J. Mod. Opt. **34**, 227 (1987).

[8]At the end of Sec. IV several integrals leading to the results for half space, symmetrical cavity, high-Q cavity, and very-narrow cavity could have been calculated analytically only by assuming that the optical parameters of the mirrors are independent of Θ. This generally leads to results that *are not* realized in real cases. Note, for instance, in Figs. 2 and 3 the large discrepancy existing, mostly for SpE inhibition, between the behavior of $\Gamma_{\parallel}(z_0)$ and $\Gamma_{\perp}(z_0)$ for the cases of ideal mirror and of real mirror, respectively. Furthermore, the large value assigned by (4.27) to $\Gamma_{\perp}$ for $d \approx 0$, in inhibition conditions, is never realized in practice as shown by Fig. 4. As a general, relevant statement, when dealing with the value and the behavior of the SpE rates, the discrepancy found by comparing the cases of ideal and real mirrors is far larger for SpE inhibition than for SpE enhancement. The expressions $r_{ij}(\Theta), t_{ij}(\Theta), \Phi(\Theta)$ have been evaluated for Ag-metal mirrors by the standard theory (Ref. 9) and plotted in Fig. 17. The computer simulation reported in the present work accounts rigorously for the Θ dependence of all optical parameters for any type of coating including metal, with the only exception of the calculations leading to Fig. 2.

[9]M. Born, and E. Wolf, in *Principles of Optics* (Macmillan, New York, 1964), Fabry-Pérot cavity thyeory, Chap. 7; optics of metals, Chap. 13. The numerical values of the complex opti-

cal parameters for the metals are found in *American Institute of Physics Handbook* (McGraw-Hill, New York, 1972), pp. 6-125 and 6-149. Unless otherwise stated, in this work all values of R_1 and R_2 are given for the mirror-air ($n = 1$) interface.

[10]R. Loudon, *The Quantum Theory of Light,* 2nd ed. (Oxford University Press, New York, 1983).

[11]H. Morawitz, Phys. Rev. **187**, 1792 (1969).

[12]M. R. Philpott, Chem. Phys. Lett. **19**, 435 (1973).

[13]G. Barton, Proc. R. Soc. London Ser. A **320**, 251 (1970).

[14]P. W. Milonni and P. L. Knight, Opt. Commun. **9**, 119 (1973).

[15]G. Barton, Phys. Scr. T **21**, 11 (1988).

[16]R. G. Hulet, E. S. Hilfer, and D. Kleppner, Phys. Rev. Lett. **55**, 2137 (1985).

[17]P. L. Knight and L. Allen, Opt. Commun. **7**, 44 (1973).

[18]*Handbook of Mathematical Functions,* edited by M. Abramowitz and I. Stegun (Dover, New York, 1965).

[19]M. Lewenstein, J. Zakrzewski, T. W. Mossberg, and J. Mostowski, J. Phys. B **21**, L9 (1988).

[20]G. Rempe, F. Schmidt-Kaler, and H. Walther, Phys. Rev. Lett. **64**, 2783 (1990).

[21]In the simulation, a more general expression of f for absorbing mirrors has been adopted (Ref. 9). There the absorption of the metal mirrors was accounted for by the dependence on Θ and polarization of the phase ϕ of the SpE reflected field; cf. Fig. 17.

[22]P. H. Lissberger, J. Opt. Soc. Am. **49**, 121 (1959); P. H. Lissberger and W. L. Wilcock, *ibid.* **49**, 126 (1959).

[23]The dielectric coatings were realized for our experiment by TVM Laboratories, Milano, and by Virgo-Optics, Port Richey, Florida. The metal coatings were realized by Instituto di Elettronica dello Stato Solido, Consiglio Nazionale delle Ricerche, Roma.

[24]P. Yeh, *Optical Waves in Layered Media* (Wiley, New York, 1988), Chap. 6; E. Yablonovich (private communication). A reduction of quantum confinement is also due, for microcavity mirrors with limited diameter, to radiation leaking in radial directions owing to the substantial thickness of dielectric coatings. Detailed computer calculations show that with our experimental dielectric mirrors this effect amounts to a $\approx 10\%$ leaking of the total energy stored in the cavity.

[25]F. De Martini, Phys. Lett. A **115**, 421 (1986), and Ref. 4; A. Kastler, Appl. Opt. **1**, 17 (1962). The "periodic pumping" technique is based on self-interference on the λ_p-reflecting mirror B, of the pump beam injected through mirror A at a selectable angle Θ_p. This technique allows one to control by Θ_p-changes the location of the "center of mass" of the distribution of excited molecules in the intracavity space in order to determine there the spatial z distribution of the energy density of the vacuum fluctuations at wavelength λ: cf. Figs. 2 and 3. A study of "periodic pumping" in the microcavity will be reported elsewhere.

[26]This f value was found to be smaller than the one obtained, under cavity excitation by a *focused* beam, by measurement of the FWHM extent $\Delta\Theta$ of the angular distribution of SpE intensity relative to the cavity forward mode: $\Delta\Theta = 2f^{-1/2}$, for $d = \bar{d}$. This last f value was found to be mostly determined by the value of $R \equiv (R_2 R_2)^{1/2}$ according to FP theory: $f = \pi R^{1/2}/(1 - R)$ (Refs. 6 and 9). There f is generally not affected by the mirror planarity but rather by properties localized within the cavity "transverse quantum-correlation length": cf. Ref. 6.

[27]C. H. Brito-Cruz, E. Palange, and F. De Martini, Opt. Commun. **39**, 331 (1981); S. Giacomini, G. Innocenti, P. Mataloni,

and F. De Martini, Appl. Opt. **26**, 3179 (1987).

[28]S. Cova, M. Bertolaccini, and C. Bussolati, Phys. Status Solidi **18**, 14 (1973).

[29]C. H. Birto-Cruz, R. L. Fork, W. H. Knox, and C. V. Shank, Chem. Phys. Lett. **132**, 341 (1986); have found that for several rhodamine dyes T_2^* is of the order of 50 fsec. The room-temperature values of the relevant characteristic times for the $^5D_0$-$^7F_2$ line of Eu-(DBM)$_4$ are $T_2^* \approx 400$ fsec, $T_0 \approx 560$ μsec. Note that with respect to SpE and to other dynamical processes considered in the present work, our microcavity operates in *steady-state* condition as its confinement time τ_{cav} is of the order of a fraction of a picosecond and then $\tau_{\mathrm{cav}} \ll T$. This justifies the adoption of the mode theory in our quantum SpE analysis.

[30]L. Derkacheva, G. Pewregudov, and A. Sokolovskaya, Usp. Fiz. Nauk **91**, 247 (1967) [Sov. Phys.—Usp. **10**, 91 (1967)]; N. Filipescu, W. F. Sager, and F. A. Serafin, J. Chem. Phys. **68**, 11 (1964); T. Kushida and E. Takushi, Phys. Rev. B **12**, 824 (1975); K. H. Drexhage, in *Progress in Optics*, edited by E. Wolf (North-Holland, Amsterdam, 1974), Vol. XII; R. Chance, A. Prock, and R. Silbey, in *Advances in Chemical Physics* (Wiley, New York, 1978), Vol. 37.

[31]N. Rehler and J. H. Eberly, Phys. Rev. A **3**, 1735 (1971).

[32]H. Kuhn and Möbius, Angew. Chem. **83**, 672 (1971); H. Kuhn, in *Physical Methods of Chemistry* (Wiley, New York, 1972), pf. III B.

[33]X. P. Feng and K. Ujihara, IEEE J. Quantum Electron **25**, 2332 (1989).